Diffuser performance analysis by measured-based modelling.

Naziema Joeman

M. Sc. Thesis

Mentor: Prof. Dr. ir. A. Gisolf
Supervisors: Dr. ir. D. de Vries
ir. M. Kuster

Delft, September 2005

Summary

Imagine a room or space where there is a sound source present creating sound that reflects at the objects present in the room (wall, chairs etc.). All reflections arriving at a listener in the room create a certain listening experience. When building a concert hall or recording room, for example, it is preferable to know how to design it such that an optimal listening experience is obtained. And when certain adjustments (objects removed, added or replaced) are made it would also be convenient to predict what the acoustical consequences are.

A routine has been set up with which these acoustical consequences of small adjustments in a space can be studied [1]. This routine starts with measuring multi-trace impulse responses of the space with for example a linear or planar array. Next, this measured data can be extrapolated to the reflecting objects or boundaries using the 'classical' wave field extrapolation theory. The extrapolation results in an image of the objects and boundaries of the space in terms of its local reflectivity. Having this information of the reflecting objects and boundaries makes it possible to make some modifications. These modifications can be: changing the reflectivity, the shape or the positions of objects or remove them entirely from the original image. When these modifications have taken place, the resulting impulse response data can be extrapolated back to the array. The acoustical differences between the modified and original space can be studied objectively in terms of energy differences and perceptually with a listening test.

This has been done last year by Kuster [1], where the reflections of a wall in a hallway were measured. An acoustical image of the wall has been made and the influence of different objects present in the hallway has been studied. With the method described above it is possible to study the performance of acoustical constructions.

In this research a Quadratic Residue Diffuser (QRD) has been modelled and was virtually placed in the hallway. A diffuser is a construction that scatters sound in different (known) directions. There are different kinds of diffusers that are based upon different mathematical number sequences. The acoustics of the hallway with the diffuser has been compared with the

acoustics of the hallway without the diffuser as described above. The energy difference of hallway with and without the diffuser showed an alternating pattern between high and low energy densities at the position of the diffuser and during the listening tests the presence of the diffuser was audible at different positions in front of the wall.

At the moment research is being done on the performance of diffusers and on quantifying this performance. Two measures are being studied: the scattering coefficient and the diffusion coefficient. The first is a measure for the amount of sound energy that is scattered away from a specific direction. The latter is a measure for the similarity between the polar response and a uniform distribution. Because of time restraints only the scattering coefficient has been calculated for the diffuser modelled in this research. At the moment research is done on the scattering of different objects in the hallway, including the diffuser modelled in this research, using these coefficients.

Samenvatting

De reflecties van objecten in een ruimte waar een bron geluid produceert, zorgen voor een bepaalde luisterervaring. Kleine veranderingen in de ruimte, zoals het verplaatsen of verwijderen van een bepaald object kunnen invloed hebben op deze luisterervaring. Het is praktisch als van tevoren voorspeld kan worden wat deze veranderingen voor gevolgen hebben voor de luisterervaring.

Dit is sinds kort op kleine schaal mogelijk door impulsresponsies te meten met een array van de te bestuderen ruimte en deze impulsresponsies vervolgens te extrapoleren naar de posities van de reflecterende objecten in de ruimte met behulp van de “klassieke” golfveldextrapolatie theorie. Het resultaat is een akoestisch beeld van de objecten in termen van de lokale reflectie.

Vervolgens is het mogelijk om met behulp van deze reflectie-informatie veranderingen aan te brengen. Dit kan bijvoorbeeld door de reflectiecoëfficiënt, de vorm of de positie van een object te veranderen of door het object geheel te verwijderen. Na het aanbrengen van de verandering is het mogelijk om de resulterende data weer te extrapoleren naar het meetarray. Het resultaat kan zowel op een objectieve als een subjectieve manier vergeleken worden met de originele meetdata van de ruimte door respectievelijk de energieverschillen te bestuderen en het afnemen van luistertests.

Bovenstaande routine is vorig jaar toegepast door Kuster [1], waarbij de impulsresponsies van een gang zijn gemeten. Met behulp van deze metingen is een akoestisch beeld van een muur in de gang gemaakt en vervolgens is de invloed op het geluid van een aantal objecten die tegen de muur geplaatst waren bestudeerd. Met bovenstaande methode is het ook mogelijk om de werking van bepaalde akoestische constructies te bestuderen.

Dat is in dit onderzoek gedaan door een Quadratic Residue Diffusor (QRD) te modelleren en virtueel in de gang te plaatsen. Een diffusor is een constructie met een specifieke vorm waarbij de vorm zo gekozen kan worden dat het geluid in specifieke, bekende richtingen verstrooid wordt. Er zijn verschillende soorten diffusoren en dus ook verschillende algoritmen waarmee deze gemodelleerd kunnen worden. De gang met de diffusor is vergeleken

met de gang met een vlakke muur op dezelfde positie. Deze vergelijking vond plaats door de energieverschillen tussen beide gangen te bestuderen en met behulp van een luistertest. Het energieverschil tussen beide gangen bestond uit een patroon van afwisselend hoge en lage energiedichtheden. Tijdens de luistertest bleek de aanwezigheid van de diffusor in de gang goed hoorbaar te zijn op verschillende posities voor de muur.

Op het moment worden twee maten bestudeerd die moeten aangeven hoe goed een diffusor het geluid verstrooit. Deze maten zijn : de scatteringcoëfficiënt en de diffusiecoëfficiënt. De scatteringcoëfficiënt is een maat voor alle geluidsenergie die van een specifieke richting af reflecteert. De diffusiecoëfficiënt geeft de werking van een diffusor aan door de polaire energiedistributie van de reflecties van een diffusor te vergelijken met een uniforme distributie. Vanwege tijdgebrek is in dit onderzoek alleen de scatteringcoëfficiënt berekend voor de gemodelleerde diffusor. Momenteel is er een onderzoek gestart waarin de scattering van verschillende objecten in de gang wordt bestudeerd met behulp van deze coëfficiënten.

Table of contents

Chapter 1
Introduction

The research described in this thesis is a follow up of earlier work done by Kuster [1]. Both investigations are based on a set of impulse responses measured in a hallway environment along a planar array of microphones. The impulse response is a registration of the pressure as a function of time at a particular source and receiver position, where the source emits an impulse. An example of the impulse response of a room at two different positions is shown in figure 1.1.

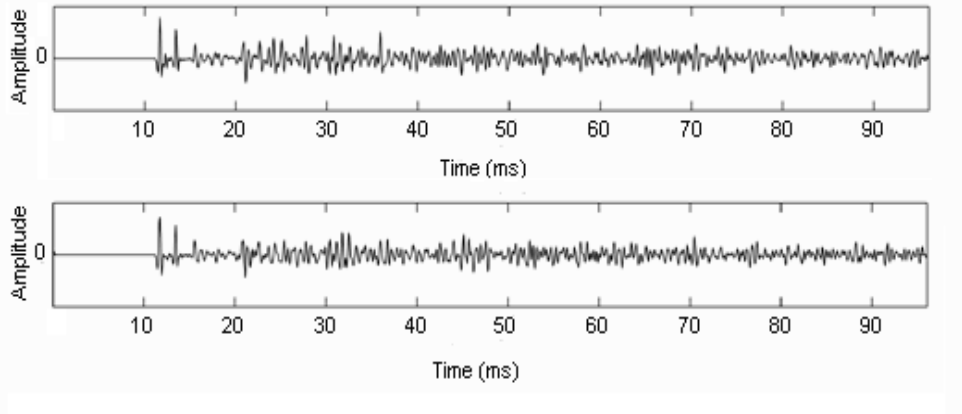

Figure 1.1: *Room impulse responses measured at a distance of* $0.5\,\mathrm{m}$ *apart.*

Within the range of the first $22\,\mathrm{ms}$ the differences between the signals are small, after that no similarity is visible. This is because during the first milliseconds the direct sound has the most influence and no or a few reflections are present, but after that the reflections start to play a bigger role. When many impulse responses are measured along a straight line, for example with a linear array, a registration can be made of the pressure as function of the travel time and offset. An example is shown in figure 1.2.

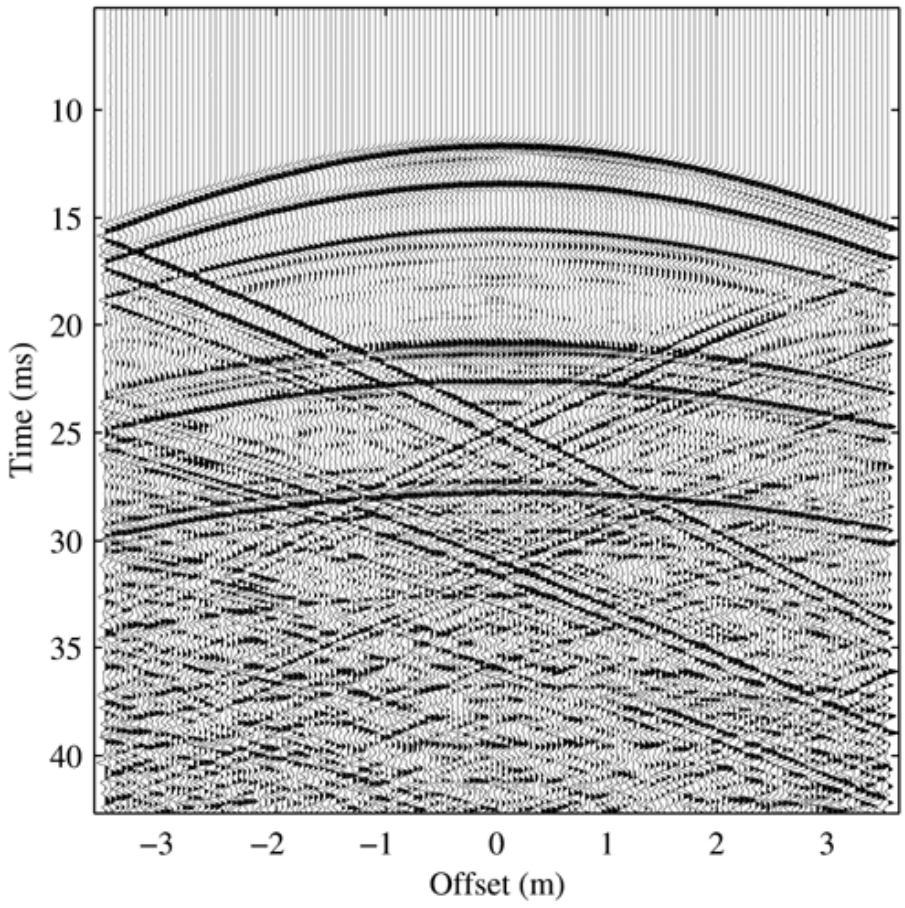

Figure 1.2: *Example of impulse responses measured along a linear array of microphone positions.*

In the figure discrete wavefronts of reflections can be identified. The correlation between the individual impulse responses is visible. The impulse response is shown at different offset-positions and at the vertical axis the travel time is shown. With the aid of the impulse responses in figure 1.2 a two-dimensional display can be made of the room boundaries [1], see figure 1.3. The easiest way to do this is by placing the linear array in such a way that it is facing a wall. It is two-dimensional because the distance between the microphones and the source or reflecting object can be calculated and measurements at different offset positions are available; there is no height information.

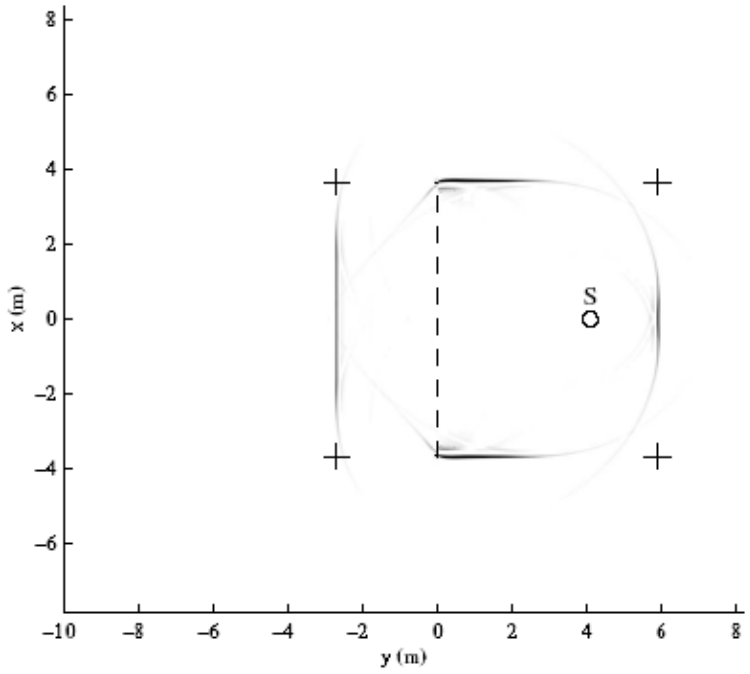

Figure 1.3: *Image of the boundaries of a room with the source and microphone array indicated by the circle and dashed line respectively. The + mark the corners of the room.*

The impulse responses dealt with in this thesis were measured in a hallway with a planar array, adding an extra dimension to the measurements. Now three-dimensional information is available in the form of distances

between source and array and offset information in the horizontal and vertical direction. This information made it possible to create a three-dimensional image of a wall in the hallway where the measurements were performed which is displayed in figure 1.4.

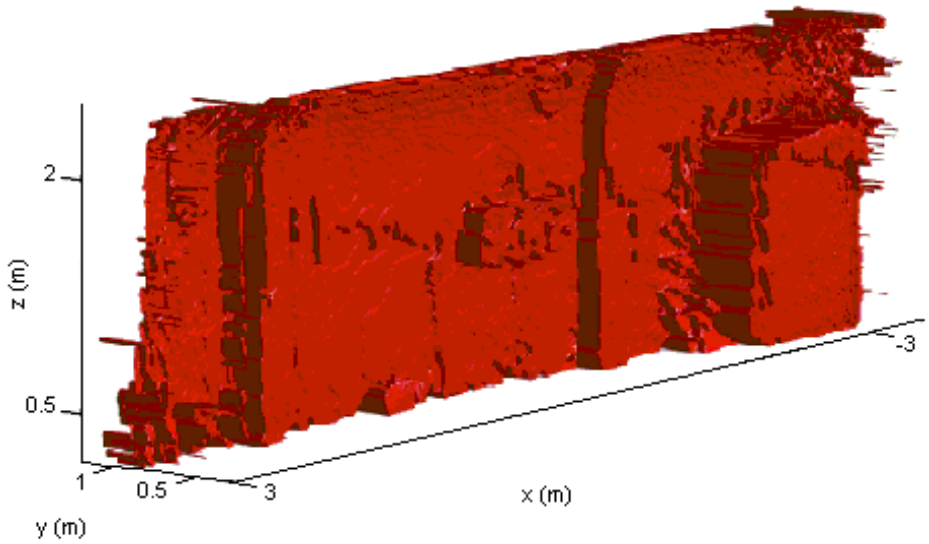

Figure 1.4: *Three-dimensional image of the wall in the hallway.*

The main goal of last years research was to map the reflections of the objects in the hallway to the reflecting objects (wall, column, fuse box etc.). This way an image of the object can be produced by only using the impulse responses of the reflections. The opposite is also possible and successful attempts have been made to convert an image into its corresponding impulse responses. This conversion made it possible to remove objects from the image and compare the acoustics of the original hallway with the acoustics of the hallway without a certain object. Removing an object was done by converting the image of the object into its corresponding impulse responses and then subtracting these from the impulse response data of the hallway. Listening tests have shown that the perceptual difference with or without a certain object is only audible in close proximity of that object.

In this thesis the above method has been used to study the performance

of a specific acoustical object: a Quadratic Residue Diffuser (QRD). First, an objective evaluation has been made by calculating the energy distribution of the hallway with and without the diffuser. The next step was a subjective evaluation by performing listening tests where the listeners had to listen to sound samples with the impulse responses of the hallway with and without the diffuser.

This thesis consists of four main parts. The first part consists of an explanation of wave field extrapolation resulting in a brief overview of the imaging routine. Next, the measurement setup and the results of Kuster's research will be presented and briefly discussed. In the second part, the theory of the quadratic residue diffuser is explained and the approach by which such a diffuser is virtually placed in the image of the hallway. In the third part the energy distribution of the diffuser and a listening test of the hallway with and without diffuser will be discussed. The fourth part will be an introduction of two new measures that quantify the performance of diffusers: the scattering coefficient and the diffusion coefficient.

Chapter 2
Imaging theory

2.1 The acoustic wave equation

A short review will be given of the theory of imaging. A more extensive explanation can be found in [1]. In the following bold letters will denote vectors, lower case letters will denote quantities in the space-time domain, upper case letters will denote quantities in the temporal Fourier domain and upper case letters with a tilde quantities in the spatial Fourier domain.

In a homogeneous isotropic medium with no losses the wave equation can be derived from two basic equations, namely Newton's second law of motion

$$-\nabla p(\mathbf{r},t) = \rho \frac{\partial \mathbf{v}(\mathbf{r},t)}{\partial t} \tag{2.1}$$

and Hooke's law for fluids

$$-\nabla . \mathbf{v}(\mathbf{r},t) = \frac{1}{K}\frac{\partial p(\mathbf{r},t)}{\partial t}. \tag{2.2}$$

By taking the divergence of equation 2.1 and combining with equation 2.2 the wave equation is obtained

$$\nabla^2 p(\mathbf{r},t) - \frac{1}{c^2}\frac{\partial^2 p(\mathbf{r},t)}{\partial t^2} = 0$$

where $c = \sqrt{\frac{K}{\rho}}$ is the speed of sound. This equation is only zero in a source free region. After Fourier transforming this equation to the frequency domain it has the following form which is called the Helmholtz equation

$$\nabla^2 P(\mathbf{r},\omega) + k^2 P(\mathbf{r},\omega) = 0 \tag{2.3}$$

where $k = \frac{\omega}{c}$ is the wave number.

For a point source represented by a delta function, equation 2.3 becomes

$$\nabla^2 P(\mathbf{r},\omega) + k^2 P(\mathbf{r},\omega) = -S(\omega)\delta(\mathbf{r}) \tag{2.4}$$

where $S(\omega)$ is the source signature. The solution is given by

$$P(\mathbf{r},\omega) = S(\omega)\frac{e^{-jk\mathbf{r}}}{\mathbf{r}}. \tag{2.5}$$

This solution represents diverging spherical waves caused by an acoustic monopole, see figure 2.1. In a similar way plane waves can be described.

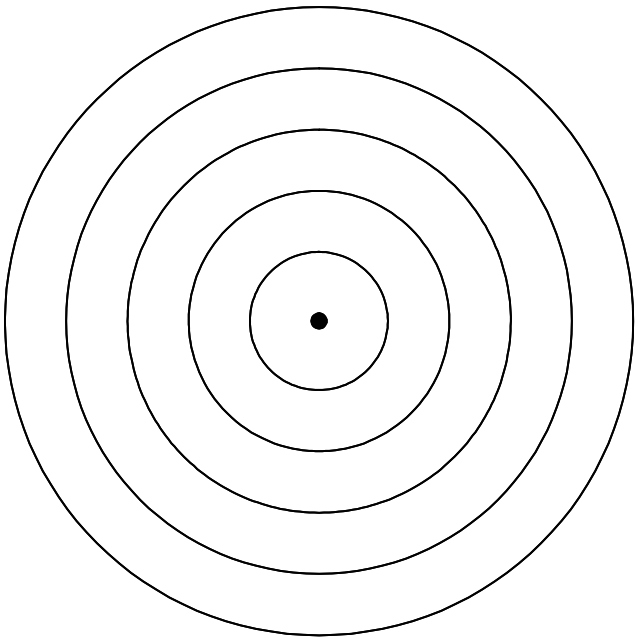

Figure 2.1: *An acoustic monopole with (spherical) wavefronts.*

Plane waves are waves where points of constant phase form planar surfaces. For the description of these waves the Helmholtz equation in the propagation direction of the wave fronts (the normal direction $\mathbf{n}$) has to be considered

$$\frac{\partial^2 P(\mathbf{r},\omega)}{\partial n^2} + k^2 P(\mathbf{r},\omega) = 0 \tag{2.6}$$

with the solution given by

$$P(\mathbf{r},\omega) = S(\omega)e^{-jk\mathbf{n}.\mathbf{r}}. \tag{2.7}$$

Unlike spherical waves, plane waves do not decay in amplitude with increasing distance.

2.2 The Kirchhoff-Helmholtz integral

Consider the second theorem of Green:

$$\int_V [f\ \nabla^2 g - g\ \nabla^2 f]\ dV = \oint_S [f\ \nabla g - g\ \nabla f].\mathbf{n}\ dS. \tag{2.8}$$

If we take for f and g solutions of the wave equation and the Green's function ($\frac{e^{-jk\Delta \mathbf{r}}}{4\pi\Delta\mathbf{r}}$) respectively, the Kirchhoff-Helmholtz integral can be derived:

$$P(\mathbf{r}_A,\omega) = \frac{1}{4\pi}\iint_S \left[P(\frac{1+jk\Delta r}{\Delta r}\cos\phi\frac{e^{-jk\Delta r}}{\Delta r}) + j\omega\rho V_n\frac{e^{-jk\Delta r}}{\Delta r}\right]\ dS. \tag{2.9}$$

Here P is the pressure on surface S generated by sources outside S (see figure 2.2), $P(\mathbf{r}_A,\omega)$ is the pressure in point A inside S, V_n is the normal component of the particle velocity, $\Delta r = |\mathbf{r}_A - \mathbf{r}_S|$ and $\cos\phi = -\frac{\partial\Delta r}{\partial n}$. For a more extensive derivation see [2].

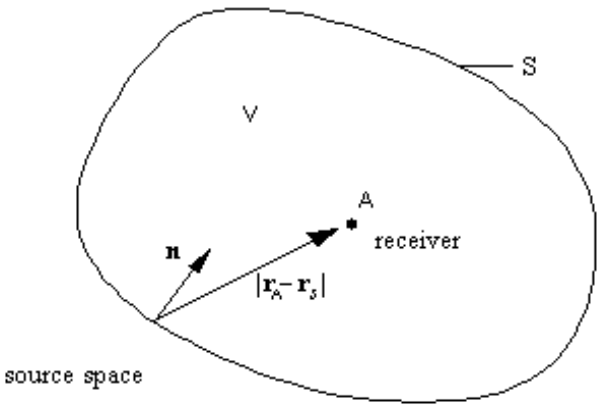

Figure 2.2: *The geometry of the Kirchhoff-Helmholtz integral.*

According to equation 2.9 the pressure in a point inside S can be calculated with the Kirchoff integral if the pressure P and the normal component of the particle velocity V_n generated by sources outside S are known on closed surface S; this is known as wave field extrapolation. With the derivation of this integral the assumption is made that V is a source free region.

Now consider the situation depicted in figure 2.3 where $z = 0$ lies on the same height as S_1 and the source is placed in the region $z < 0$. If the surface

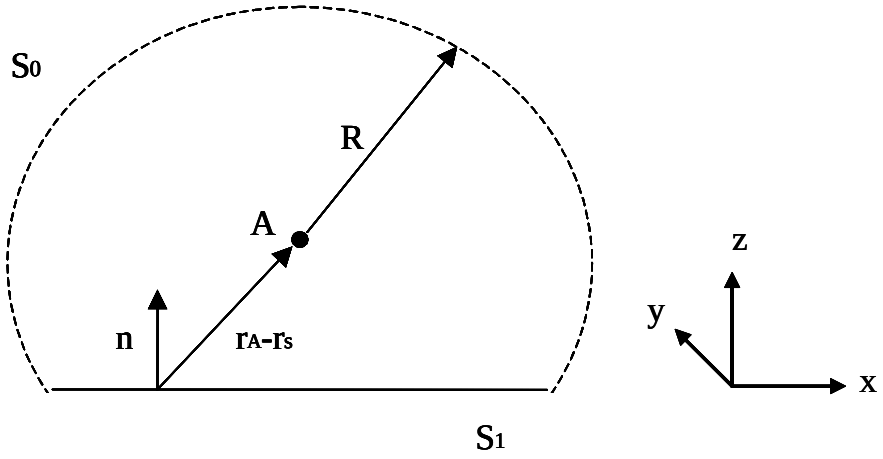

Figure 2.3: *Closed surface S for the derivation of the Rayleigh integrals.*

S is composed of surfaces S_0 and S_1, then the pressure in point A is given by the contribution of two surface integrals, namely over S_0 and S_1. Now, if we let $R \to \infty$ then the contribution of surface S_0 will vanish and only the contribution of the plane surface S_1 will be needed to calculate the pressure in A:

$$P(\mathbf{r}_A, \omega) = \frac{1}{4\pi} \int_{-\infty}^{\infty} \int_{-\infty}^{\infty} P(x, y, z, \omega)\left(\frac{1 + jk\Delta r}{\Delta r} \cos\phi \frac{e^{-jk\Delta r}}{\Delta r}\right) + j\omega\rho V_n(x, y, z, \omega) \frac{e^{-jk\Delta r}}{\Delta r}\, dxdy. \tag{2.10}$$

It is shown in [2] that in this situation the Kirchoff integral can be written as a sum of two integrals, the Rayleigh I and Rayleigh II integrals. Rayleigh I consists of the first part of the integrand in equation 2.10 and Rayleigh II of the second. Only one of these integrals is required to calculate the pressure

P_A in point A. Rayleigh I reads:

$$P(\mathbf{r}_A, \omega) = \frac{1}{2\pi} \int_{-\infty}^{\infty} \int_{-\infty}^{\infty} j\omega\rho V_n(x, y, z = 0, \omega) \frac{e^{-jk\Delta r}}{\Delta r} dxdy. \tag{2.11}$$

Rayleigh I expresses the pressure in point A, as a weighted sum of *the normal component of the particle velocity* on the plane S_1. Rayleigh II has the following form:

$$P(\mathbf{r}_A, \omega) = \frac{1}{2\pi} \int_{-\infty}^{\infty} \int_{-\infty}^{\infty} P(x, y, z = 0, \omega)(\frac{1 + jk\Delta r}{\Delta r}) \cos\phi \frac{e^{-jk\Delta r}}{\Delta r} dxdy \tag{2.12}$$

where $\cos\phi = \frac{\Delta z}{\Delta r}$. Rayleigh II expresses P_A as a weighted sum of *the pressure* on S_1.

2.3 Forward and inverse wave field extrapolation

With equations 2.11 and 2.12 the pressure in a point (A) in a source free volume can be calculated when the pressure or the normal component of the particle velocity on a plane (S or S_1) are known. The calculation of the pressure in points in the direction of the propagation of the wave field is called forward wave field extrapolation. When the pressure on the plane S_1 is known and the pressure in the direction *against* the propagation direction of the wave field has to be calculated, this is referred to as inverse wave field extrapolation. In the research of this thesis the reflection boundary of interest was on one side of the array and the source on the other so, both forms of wave field extrapolation were used, namely, from the array to the wall (inverse) and from the wall to the array (forward). This will be further explained in the following.

2.4 Imaging routine

By inverse Fourier transformation of equation 2.9 the equation used to calculate the image points in the time domain is obtained. The integral can be written in a compact form with elements W_{1I} and W_{2I}, which are defined by

equations 2.13 and 2.14.

$$W_{1I}\left(\mathbf{r}_I, \mathbf{r}_R, t\right) = \rho_0 \frac{1}{4\pi r_{IR}} \frac{\partial}{\partial t}, \tag{2.13}$$

$$W_{2I}\left(\mathbf{r}_I, \mathbf{r}_R, t\right) = \frac{\cos\phi}{4\pi r_{IR}} \left(\frac{1}{r_{IR}} - \frac{1}{c} \frac{\partial}{\partial t} \right). \tag{2.14}$$

Here $\mathbf{r}_R$ is the position vector of a receiver with three cartesian components $(r_{R_x}, r_{R_y}, r_{R_z})$ and $\mathbf{r}_I$ is the position vector of the image point I. Using W_{1I} and W_{2I} the integral equation has the following form

$$\begin{aligned} \langle p_{\mathrm{Im}}(\mathbf{r}_I) \rangle \quad = \quad & \iint dr_{R_x} dr_{R_z} [W_{1I}\left(\mathbf{r}_I, \mathbf{r}_R, t\right) v_n(\mathbf{r}_R, t) + ... \\ & W_{2I}\left(\mathbf{r}_I, \mathbf{r}_R, t\right) p(\mathbf{r}_R, t)] \mid_{t=\tau(\mathbf{r}_S, \mathbf{r}_I, \mathbf{r}_R)} \end{aligned} \tag{2.15}$$

where

$$\tau(\mathbf{r}_S, \mathbf{r}_I, \mathbf{r}_R) = \frac{r_{SI} + r_{IR}}{c}$$

In equation 2.15 $p_{\mathrm{Im}}(\mathbf{r}_I)$ is the image at point I in terms of the reflected pressure, $p(\mathbf{r}_R, t)$ and $v_n(\mathbf{r}_R, t)$ are the measured pressure and normal component of the particle velocity on the planar array respectively. Furthermore, r_{SI} is the distance from source to image point and r_{IR} is the distance from image point to receiver (see figure 2.4) which makes τ the travel time from the source S to receivers $\mathbf{R}$ $(= (r_{R_x}, r_{R_z}))$.

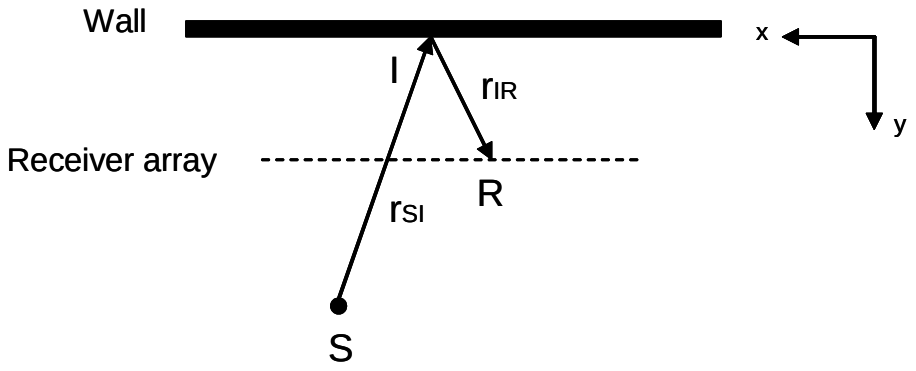

Figure 2.4: *Geometry for the imaging with source S, image point I and receiver array.*

The imaging routine is as follows: first the pressure and particle velocity are measured on the array; both are inverse extrapolated to point I with W_{1I} and W_{2I}; next, the travel time from source S to image point I is calculated ($\frac{r_{SI}}{c}$) and the extrapolated pressure amplitude at this time is used as image information p_{Im}. These steps are repeated for all points I in the region.

Which integral is used for the calculation of the image points is dependent on the available information. When only the pressure is available the Rayleigh II integral is used for the imaging process which was the case in this research. The Rayleigh II integral in the time domain reads:

$$\langle p_{\mathrm{Im}}(\mathbf{r}_I)\rangle = 2\iint dr_{R_x} dr_{R_z} W_{2I}\left(\mathbf{r}_I, \mathbf{r}_R, t\right) p(\mathbf{r}_R, t)|_{t=\tau(\mathbf{r}_S,\mathbf{r}_I,\mathbf{r}_R)} \tag{2.16}$$

After imaging the next step is the alteration of objects. This is done by first transforming the image points of the object to be altered back into impulse responses and forward extrapolation to the array. Transforming the image points to impulse responses is done by integrating over the image points in space. The integral equation including forward extrapolation to the array reads:

$$\langle p(\mathbf{r}_R, t)\rangle = \iint dr_{I_x} dr_{I_z} W_{2F}\left(\mathbf{r}_R, \mathbf{r}_I, t\right) p_{\mathrm{Im}}(\mathbf{r}_I)|_{r_{I_y}=\psi(\mathbf{r}_S, r_{I_x}, r_{I_z}, \mathbf{r}_R, t)} \tag{2.17}$$

where

$$W_{2F}\left(\mathbf{r}_R, \mathbf{r}_I, t\right) = \frac{\cos\phi}{4\pi r_{IR}}\left(\frac{1}{r_{IR}} + \frac{1}{c}\frac{\partial}{\partial t}\right) \tag{2.18}$$

and again

$$t(\mathbf{r}_S, r_{I_x}, r_{I_y} = \psi(\mathbf{r}_S, r_{I_x}, r_{I_z}, \mathbf{r}_R, t), r_{I_z}, \mathbf{r}_R) = \frac{r_{SI} + r_{IR}}{c}$$

For the *removal* of an object the impulse responses of the object have to be subtracted from the original impulse responses of the hallway (alteration). Of the changed impulse responses an image can be made with equation 2.16 (re-imaging). It is of course also possible to add objects and thus replace a specific object with another object. This is done by subtracting the impulse responses of the object and simultaneously adding the impulse responses of the other object at the same positions. The combination of converting image

points back to impulse responses and forward extrapolation to the array is called demigration.

The whole routine including alteration of objects and re-imaging of the hallway is explained according to the schematic diagram displayed in figure 2.5.

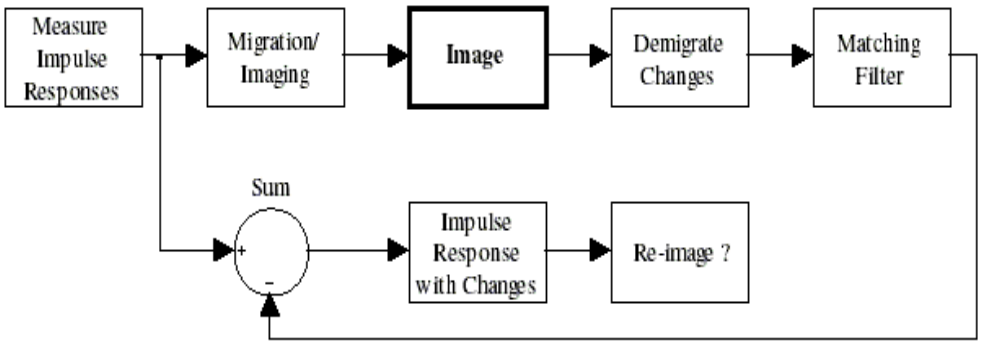

Figure 2.5: *Schematic diagram of the alteration of the image of the hallway.*

- The impulse responses are measured on the array.
- These impulse responses are inverse extrapolated to the wall and converted into image points, which is called migration.
- A total image of the wall is made.
- The image of the object to be altered is converted into its impulse responses and forward extrapolated to the array.
- A matching filter is applied, because the demigration step causes some alterations in the phase and amplitude.
- The impulse responses of the object are subtracted from the original impulse responses and re-imaging takes place.

The measurement set up and the results of Kuster's research are discussed in the next chapter.

Chapter 3
Measurements and imaging

3.1 Measurement set up

A picture of the hallway where the measurements were performed is shown in figure 3.1. The hallway has a height of $3.37\,\mathrm{m}$ and a width of $3.56\,\mathrm{m}$. The receiver array consisted of cardioid microphones and was placed in front of the wall shown in figure 3.1. Visible are a fuse box, two columns, a closet etc.

Figure 3.1: *Picture of the hallway.*

As mentioned before, Kuster's measurements were done with a planar array. The array was $7\,\mathrm{m}$ long and $2.5\,\mathrm{m}$ high and was placed at a distance of $0.88\,\mathrm{m}$ in front of the wall. The source was placed behind the array and the shortest distance between the array and the source was $1.68\,\mathrm{m}$. The origin of the coordinate system lies at the centre of the lower edge of the array which is at a height of $0.35\,\mathrm{m}$ above the floor. A schematic view is shown in figure 3.2.

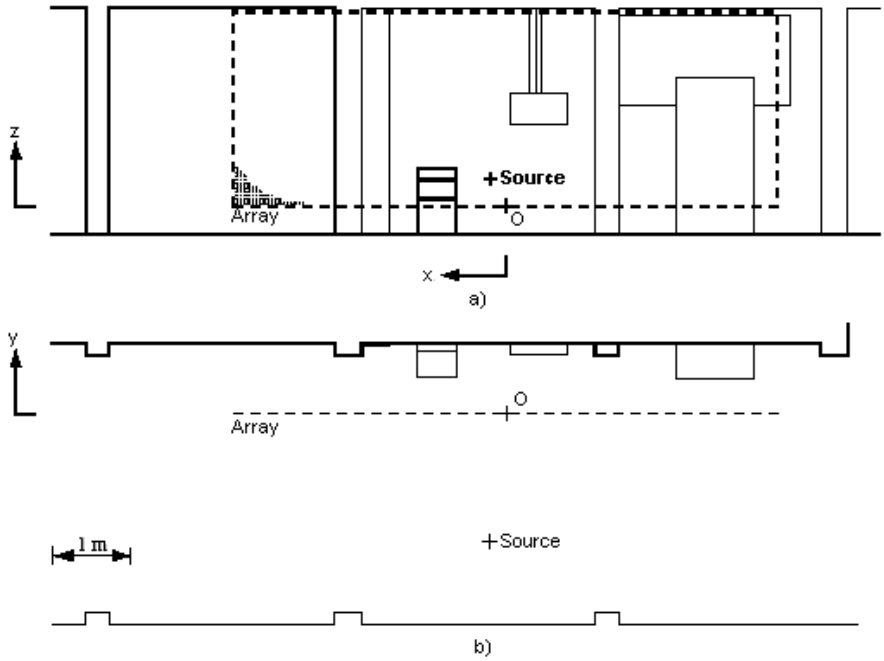

Figure 3.2: *a) A view from the front and b) a floorplan of the hallway.*

The sampling distance in the horizontal and vertical direction was $0.05\,\mathrm{m}$ and thus there was a total of 7000 measurement points.

3.2 Imaging

The part of the measured impulse responses containing the reflections of the wall in the hallway is shown in figure 3.3. The reflection of the fuse box is indicated by the black box and the primary and secondary reflections of the closet are indicated by the arrows. Also visible are the hyperbola in the top of

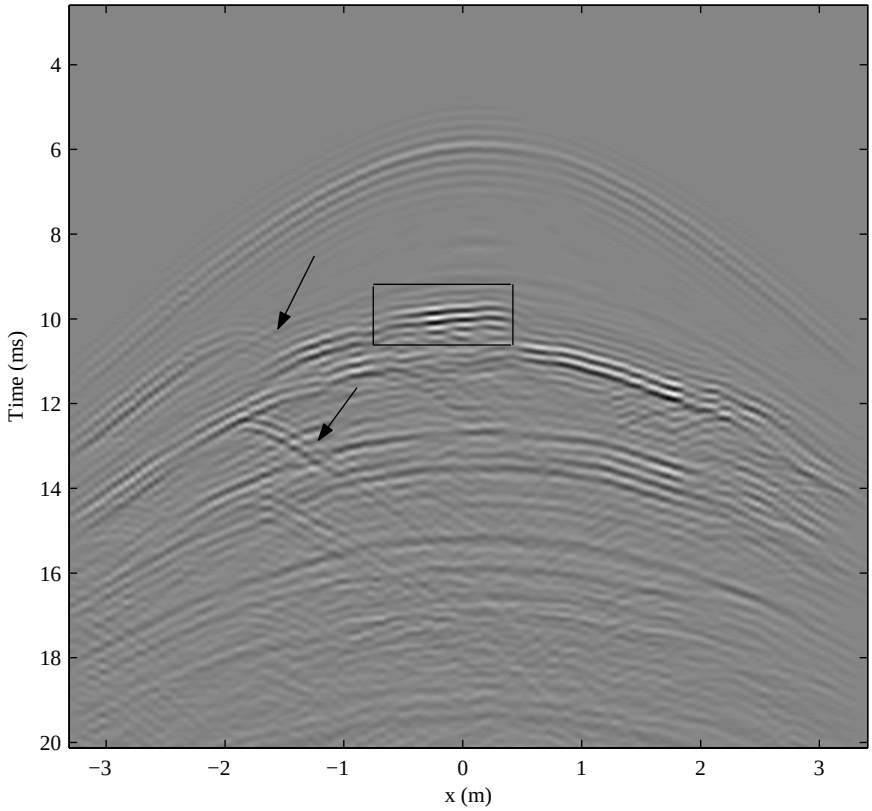

Figure 3.3: *The multi-trace impulse response of the hallway at height* $z = 1.5\,\mathrm{m}$.

the figure, which is the attenuated direct sound and the multiple reflections which are caused by sound that is reflected from the back wall. The impulse responses can be converted into image points as explained in section 2.4. For the imaging only the primary reflections of the wall including objects are needed, however in figure 3.3 the direct sound and the reflections coming from the back wall are also present. Prior to the imaging the time window in which the primary reflections arrived at the array is determined and only this information is used in the imaging process (see figure 3.4; only the reflections between the two white hyperbolas are used for imaging). This way the direct sound and the reflections coming from the back wall are 'eliminated'.

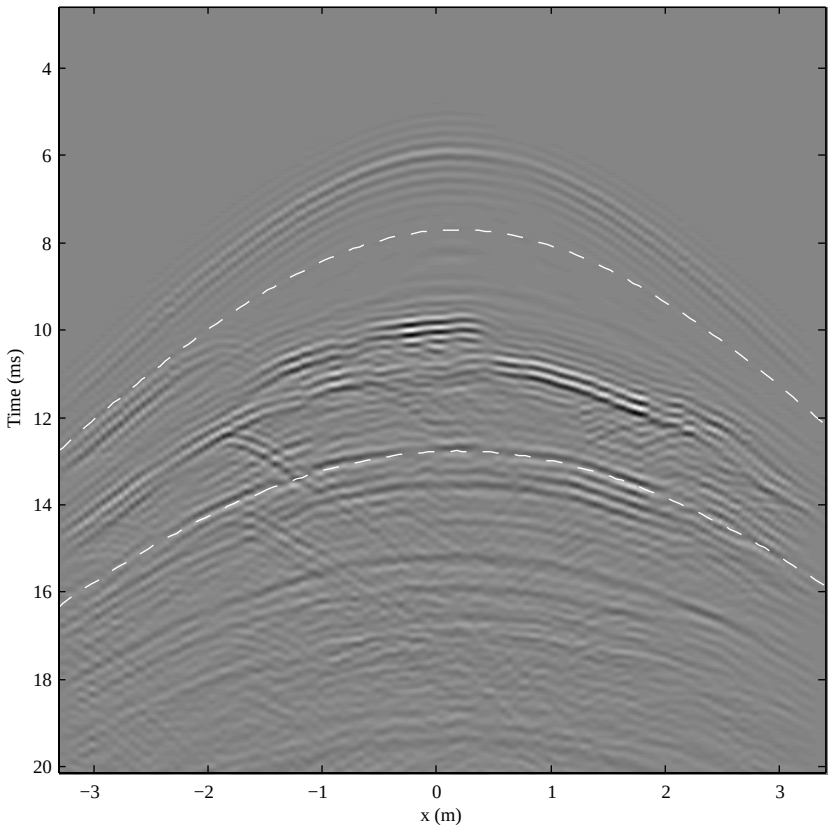

Figure 3.4: *Two white hyperbolas indicating the parts of the multi trace impulse response that is used for imaging.*

The image can be displayed in two different ways. First, it is possible to

make horizontal image slices of the wall at fixed heights. Horizontal slices of the wall are displayed in figure 3.5 at three different heights.

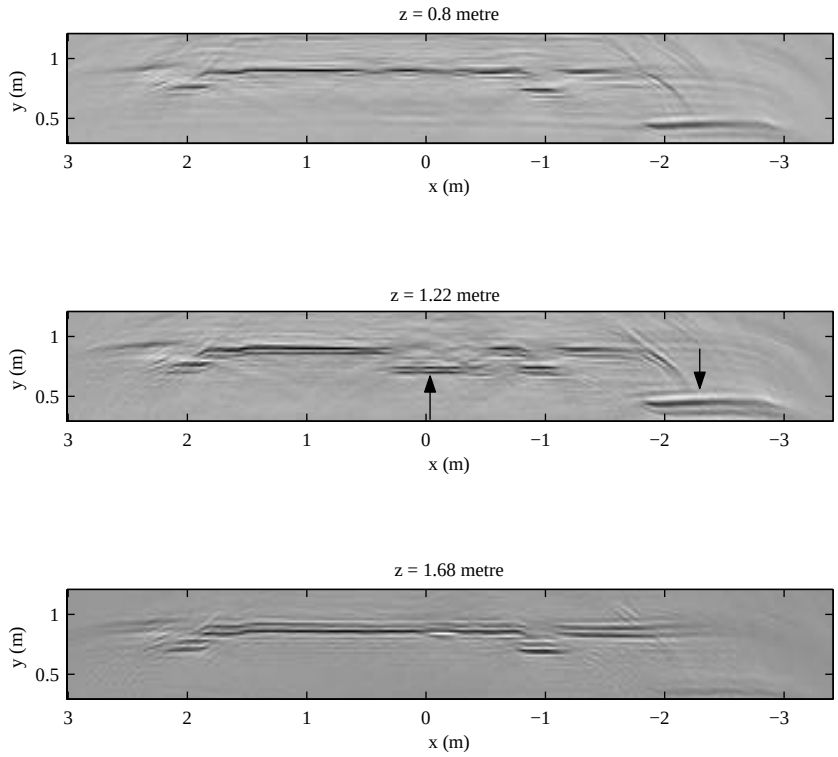

Figure 3.5: *Image slices of the wall at three different heights.*

In the second slice, at $z = 1.22\,\mathrm{m}$, in figure 3.5 the fuse box and the closet are indicated with arrows. In the top slice the closet is also visible whereas the fuse box is not, because the height $z = 0.8\,\mathrm{m}$ is below the position of the fuse box. Also clearly visible are the two columns at $x = -1\,\mathrm{m}$ and $x = 2\,\mathrm{m}$.

The second way to display the wall is by making a three-dimensional image of the entire wall with objects. The three-dimensional image is displayed in figure 3.6. In figure 3.6 the position and size of the objects are clearly visible. During the measurements a chair was placed against the wall in the hallway. The chair was not present when the picture in figure 3.1 was taken, but it is visible in figure 3.6 and indicated by the black arrow. The three-dimensional image is a nice result where the entire wall, including all

objects, are visible, but by making horizontal slices the objects can also be clearly recognized and it takes much less processing time than making a three-dimensional image. A more extensive discussion of these results can be found in [1].

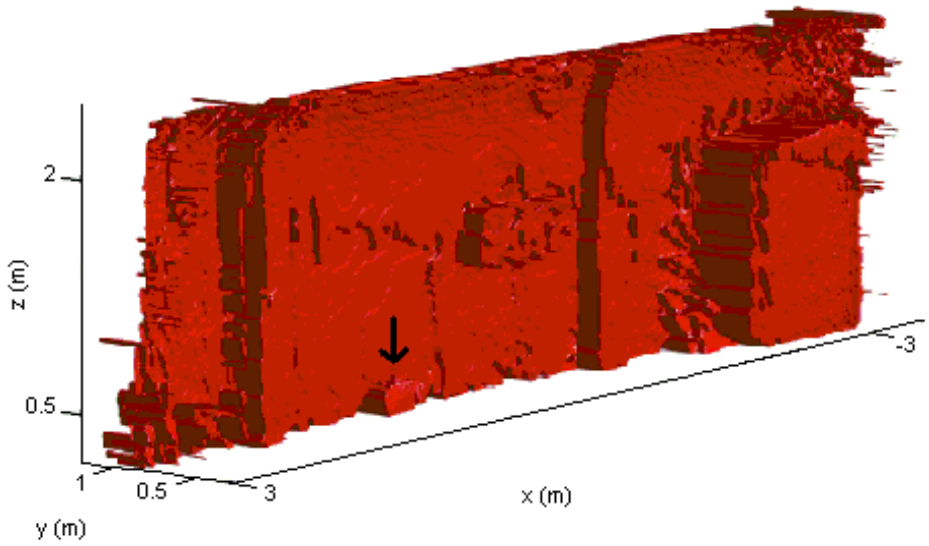

Figure 3.6: *Three-dimensional image of the wall.*

3.3 Demigration and re-imaging

In Kuster's research the fuse box and the closet were removed from the image. This was done by demigrating the objects and subtracting their impulse responses from the total impulse response data of the hallway and thus leaving holes at the original positions of the fuse box and the closet.

The present research started with an attempt to replace the fuse box by a flat surface. The result is displayed in figure 3.7.

By comparing this image with the image in figure 3.6 it is seen that between the two columns there is now a flat wall. The irregularities at $z = 2.0\,\mathrm{m}$ and higher are caused by the fact that this area is outside the range

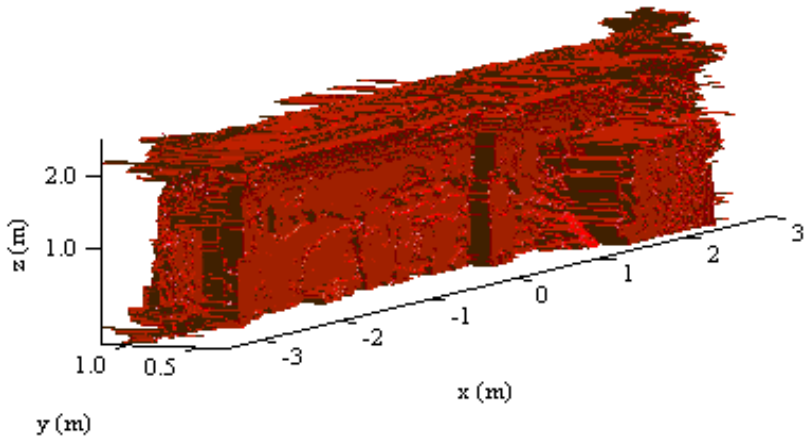

Figure 3.7: *Three-dimensional image of the wall where the fuse box is replaced by a flat piece of wall.*

of the planar array. This means that for that area there is not enough reflection information, because many reflections do not reach the array but travel over the array. The impulse response containing the reflections of the wall in figure 3.7 is displayed in figure 3.8. When comparing this figure with figure 3.3, the difference is visible in the areas indicated by the black boxes.

After this successful attempt the next step was to model a quadratic residue diffuser and place it in the hallway. This will be the main focus in the remainder of this thesis.

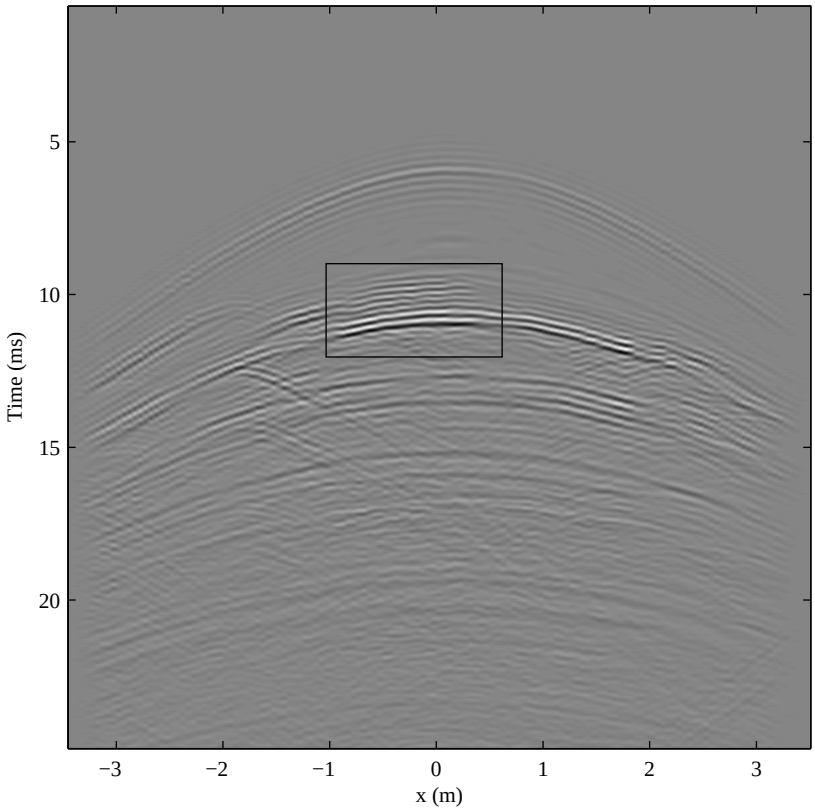

Figure 3.8: *Multi-trace impulse response of the wall in the situation where the fuse box is replaced by a flat piece of wall.*

Chapter 4
Sound diffusion

There are many factors that affect the acoustics of a room. For example, the dimensions of the room, the reflective and absorptive properties of the walls and other surfaces present in the room. In Kuster's thesis [1] the reflections were of primary importance and in this thesis they still are, but the effect of sound diffusion in particular. Especially in concert halls and recording studios much use is made of different kinds of diffusers. The contribution of diffusers to sound perception is the sense of spaciousness: they make the sound more stereophonic and less monophonic. One of the most important causes of this is the effect of binaural dissimilarity which will be discussed first, followed by the basics of diffuser performance.

4.1 Binaural Dissimilarity

The requirement of binaural dissimilarity, necessary for perception of spaciousness, means that the signals received at the two ears of a listener should be as uncorrelated as possible. This uncorrelation gives the listener the impression of being 'immersed' in the sound, a feeling of spaciousness. Sound that arrives in the vertical symmetry plane through the head (from the front to the back of the head) results in a similar sound pressure at the two ears. As a consequence the listener has a rather 'flat' or monophonic sound, no sense of spaciousness. Primary reflections from the ceiling and the front and back walls of a hall result in such sound and therefore do not contribute to the spaciousness of sound [3].

The reflections from plane walls and ceilings are specular and can be useful for the intelligibility and the "presence" (the feeling that the stage and hall are an acoustic entity) of sound. But often it is preferred that sound impinging from one particular direction on a wall of a hall is scattered in many different directions, because it results in lateral reflections arriving at the

listeners two ears with different travel times and amplitudes causing binaural dissimilarity. In a concert hall the listeners are formed by the audience as well as the performers on stage. It is impossible to create binaural dissimilarity for the whole audience (in the front and back) with specular reflections only. This is where diffusers provide a solution and not only by creating more lateral reflections. The (diffuse) reflections from the diffuser from other directions than the lateral direction also arrive with different travel times at the ears of the listener and thus also contribute to binaural dissimilarity.

4.2 The Quadratic Residue Diffuser

A diffuser is a construction that scatters sound in different directions. When a sound wave impinges on a diffuser, the diffuser scatters the wave into a number of 'wavelets' over a wide angular distribution. A distinction can be made between diffusers that scatter in the horizontal and in the vertical direction. However, a combination of both is also possible, see figure 4.1. In this figure two diffusers are shown consisting of little wells. When the depth of the wells vary only in the horizontal direction the diffuser scatters in the horizontal direction and when the depth varies in the vertical direction the diffuser scatters the sound in the vertical direction. When the depth of the wells varies in both directions it scatters in both directions. Nowadays there are different methods to develop a diffuser and, hence, there is a wide variety of diffusers [4]. One of those is the Quadratic Residue Diffuser (QRD) of which a one-dimensional version is investigated in this research.

The QRD was developed by Schroeder [5] and is described as a surface in which there are a number of narrow ($< \frac{\lambda}{2}$) wells of different depths. The principle is as follows: when sound waves impinge on the diffuser, plane waves are propagating in each well. Dependent on the depth of each well and, hence, the distance the wave travels in the well, a certain phase change takes place between incident and reflected wave. The phase change $\Delta\phi$ is given by

$$\Delta\phi = \omega\Delta t$$

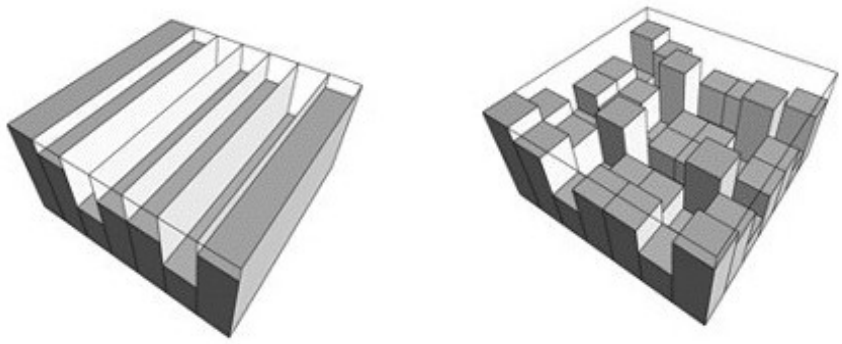

Figure 4.1: *Examples of a 1-dimensional and a 2-dimensional diffuser on the left and right respectively.*

where ω is the frequency of the sound wave and Δt is the travel time difference. So the phase differences occurring in each well are caused by the travel time differences which on their turn are caused by the different distances the waves travel inside the wells. The different phase changes caused by the varying depths of the wells result in different local reflection coefficients. Because of these different local reflection coefficients a plane wave impinging from one direction will be (equally) scattered in different directions; an example is shown in figure 4.2. A further (mathematical) explanation is given in the following subsections. More about the scattering from quadratic residue diffusers can be found in [6], [7] and [8].

4.2.1 Theory

The QRD is based on a mathematical number sequence, called the quadratic residue sequence of elementary number theory. Such a sequence is periodic and defined as follows

$$s_n = n^2 \bmod N \tag{4.1}$$

where N is a prime number, $n = 0, 1, 2, ...$ and hence, s_n is the residue after taking the long division by N. For $N = 7$, for example, $n^2 = 0, 1, 4, 9, 16, 25, 36, 49, 64, ...$ and $s_n = 0, 1, 4, 2, 2, 4, 1, 0, 1, ...$ The

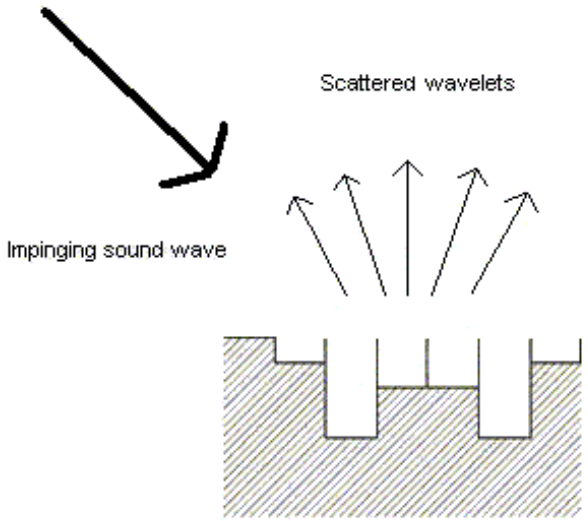

Figure 4.2: *A sound wave scattering on a diffuser.*

upper boundary for s_n is $s_{\max} = N - 1$. These sequences are periodic with period N and are symmetric around $s_n = 0$ and around the dividing line between the two middle elements within one period excluding 0.

Fourier The theory of QRD's will be described in the spatial Fourier domain. The spatial Fourier domain is analogous to the temporal Fourier domain. Just as the temporal Fourier transformation decomposes an array recording $f(x,t)$ into sines with different frequencies ω for each position x resulting in a dataset $F(x,\omega)$, the spatial Fourier transformation decomposes this function $F(x,\omega)$ into sinusoidal spatial functions for each ω. These sinusoidal spatial functions for a fixed ω represent the projection of plane waves incident from different directions on the recording array. The mathematical analogy is explained below.

***Temporal Fourier transform*: time** (t) $\underrightarrow{\text{FT}}$ **frequency** $(f$ **or** $\omega)$

When taking a signal $f\ (x,t) = f_x(t)$ the temporal Fourier transformation is

defined by

$$F_x(\omega) = \int_{-\infty}^{\infty} f_x(t) e^{-j\omega t} dt \tag{4.2}$$

and the inverse Fourier transformation of $F_x(\omega)$ by

$$f_x(t) = \frac{1}{2\pi} \int_{-\infty}^{\infty} F_x(\omega) e^{+j\omega t} d\omega \tag{4.3}$$

For discrete periodic signals these equations are given by

$$F_x[\omega_m] = \sum_{n=0}^{N-1} f_x\,[t_n] e^{-j\omega_m t_n} \tag{4.4}$$

$$f_x\,[t_n] = \frac{1}{N} \sum_{m=0}^{M-1} F_x[\omega_m] e^{+j\omega_m t_n} \text{ or } f_x\,[t_n] = \frac{1}{N} \sum_{m=0}^{M-1} F_x[\omega_m] e^{+j2\pi \frac{m}{T} t_n} \tag{4.5}$$

F_x is the amplitude of the $m'th$ harmonic, $\omega_m = \frac{2\pi m}{T}$ is the $m'th$ frequency sample and T the period of the signal.

***Spatial Fourier transform*: space (x) $\underset{\rightarrow}{\text{FT}}$ spatial frequency (k_x)**

When rearranging signal $F_x(\omega)$ to $F_\omega(x)$, the spatial Fourier transformation is defined as

$$\widetilde{F_\omega}(k_x) = \int_{-\infty}^{\infty} F_\omega(x) e^{+jk_x x} dx \tag{4.6}$$

and the inverse transformation of $\widetilde{F_\omega}(k_x)$ is given by

$$F_\omega(x) = \frac{1}{2\pi} \int_{-\infty}^{\infty} \widetilde{F_\omega}(k_x) e^{-jk_x x} dk_x \tag{4.7}$$

with k_x (the spatial frequency) the x-component of the wave number $\mathbf{k}$. Again there is a discrete form of the continuous equation given above

$$\widetilde{F_\omega}[k_{x_m}] = \frac{1}{N} \sum_{n=0}^{N-1} F_\omega\,[x_n] e^{+jk_{x_m} x_n} \tag{4.8}$$

$$F_\omega\,[x_n] = \sum_{m=0}^{M-1} \widetilde{F_\omega}[k_{x_m}]e^{-jk_{x_m}x_n} \text{ or } F_\omega\,[x_n] = \sum_{m=0}^{M-1} \widetilde{F_\omega}[k_{x_m}]e^{-j2\pi\frac{m}{L}x_n} \tag{4.9}$$

$\widetilde{F_\omega}$ is the amplitude of the $m'th$ spatial harmonic, k_{x_m} the $m'th$ spatial frequency sample and L the period of the signal.

According to Cox and d'Antonio [9] the pressure magnitude for one-dimensional scattering from a source via surface (s) to a receiver is given by

$$|p(\theta,\psi)| \approx \left| C \int_s R(x,\omega) e^{jkx[\sin(\theta)+\sin(\psi)]} dx \right| \tag{4.10}$$

which has a similar form as the Fourier Transform given in equation 4.6. Here $R(x,\omega)$ is the reflectivity factor, θ the angle of reflection, ψ the angle of incidence, k the wavenumber and C a constant. The derivation is given in [9] in chapters 8 and 9. For a periodic surface there will be scattering directions where the path length difference from source to receiver, via points on the surface that are exactly one period apart, will be a multiple of the wavelength. In these directions there will be constructive interference and periodicity lobes will occur. The directions in which these lobes occur in the far field can be calculated with the aid of figure 4.3 where the path length difference $r1 + r3 - r2 - r4 = m\lambda$ for pressure maxima, where $m = 0, \pm1, \pm2$ etc. is the order of the lobes and λ is the wavelength of the impinging wave. These directions are given by [9]:

$$\sin(\theta_m) = \frac{m\lambda}{L} - \sin(\psi) \tag{4.11}$$

where L is the length of one period. From this equation follows that

$$\theta_m = \arcsin(\frac{m\lambda}{L} - \sin\psi) \tag{4.12}$$

where for propagating waves:

$$\left| \frac{m\lambda}{L} - \sin\psi \right| \leq 1. \tag{4.13}$$

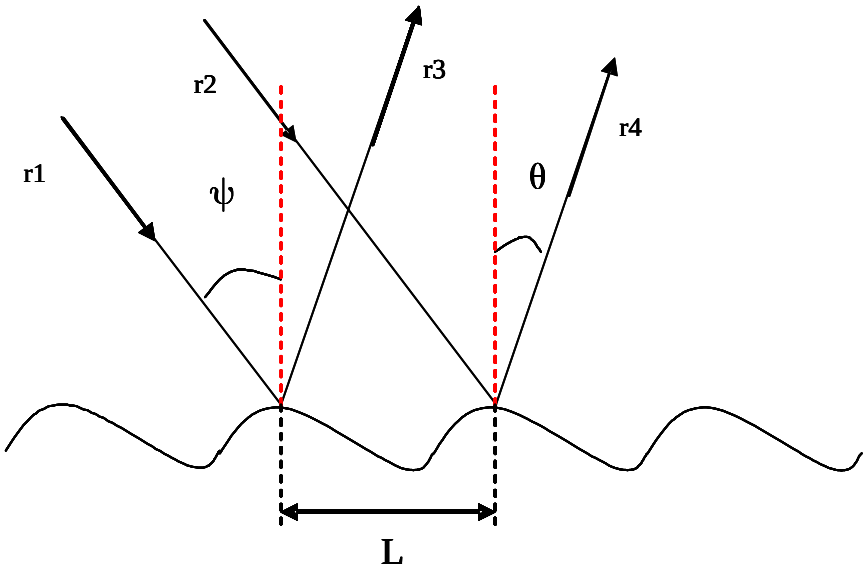

Figure 4.3: *Illustrative scheme with which the path length difference can be calculated.*

$\left|\frac{m\lambda}{L} - \sin\psi\right| > 1$ represents evanescent waves. These waves diminish exponentially with distance and therefore are only present in the near field. For normal incidence on the reflecting surface the non-evanescent scattering angles θ_m can vary from $-90°$ to $+90°$ (where $0°$ corresponds to the direction normal to the reflecting surface).

From inequality 4.13 follows that when ψ is fixed, m can take on higher values when the wavelength λ decreases (and thus the frequency f increases) and thus at higher frequencies there will be a higher amount of scattering lobes. In equation 4.11 it can be seen that $m = 0$ corresponds to the specular reflection: $\sin(\theta_0) = -\sin(\psi) \Longrightarrow \theta_0 = -\psi$. For a specific surface the first scattering lobe that is not the specular reflection occurs at the lowest value of m for which the inequality 4.13 is still valid; this is at $m = 1$ or $m = -1$ or both, dependent on the angle of incidence and the wavelength of the impinging wave. As an example normal incidence $(\psi = 0)$ and $\psi = 90°$ will be considered. For normal incidence equation 4.12 becomes:

$$\theta_m = \arcsin(\frac{m\lambda}{L}) \tag{4.14}$$

From this equation can be seen that the scattering lobes are symmetrically distributed around the angle of incidence ($0°$). For normal incidence the first scattering lobe is given by:

$$\theta_{\pm 1} = \arcsin(\frac{\pm\lambda}{L}) \tag{4.15}$$

with $\left|\frac{\pm\lambda}{L}\right| \leq 1 \Longrightarrow \frac{\lambda}{L} \leq 1$, because λ and L are always positive. From this inequality follows that $\lambda \leq L$. For the second (order) scattering lobe: $\frac{2\lambda}{L} \leq 1$. This scattering lobe does not occur when $\lambda > \frac{L}{2}$. So, as long as $\frac{L}{2} < \lambda \leq L$ there will be only one scattering lobe at each side of the specular reflection (for $m = +1$ and $m = -1$), see figure 4.4.

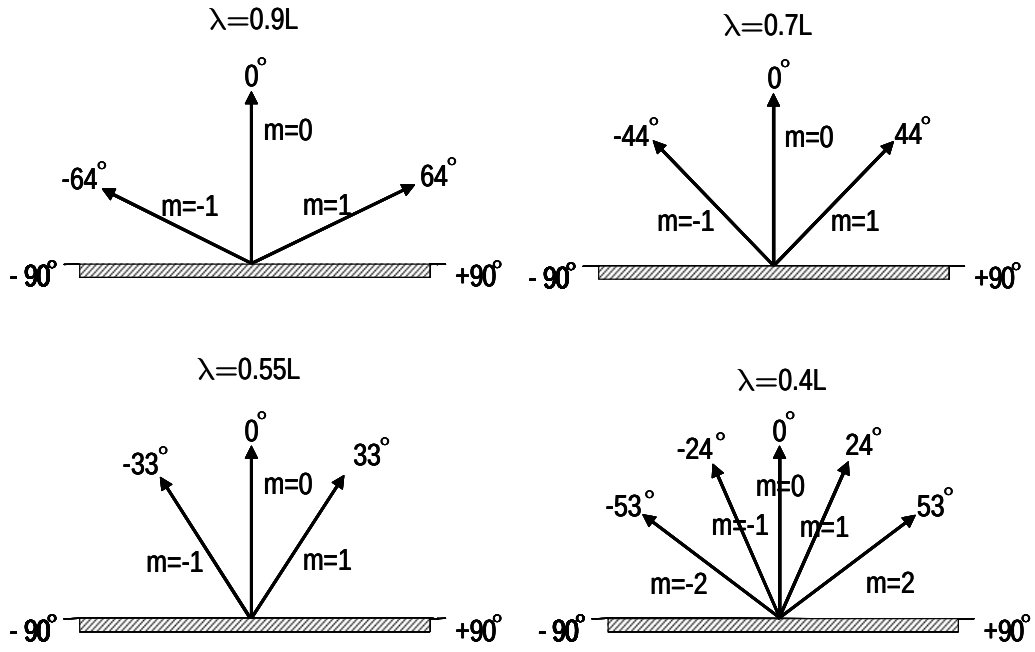

Figure 4.4: *Illustration of the relation between the amount of scattering lobes and the wavelength at an angle of incidence of* $0°$.

This can be extended to the $m'th$ lobe; for the $m'th$ lobe: $\frac{m\lambda}{L} \leq 1$, so there will be $m-1$ lobes at each side of the specular reflection if $\frac{L}{m} < \lambda \leq L$. For

$m = \pm 1$ and $\psi = 90°$ equation 4.12 becomes:

$$\theta_{\pm 1} = \arcsin(\frac{\pm\lambda}{L} - 1) \tag{4.16}$$

Since λ and L are positive and $\left|\frac{\pm\lambda}{L} - 1\right| \leq 1$, m can only be $+1$. There will be only one scattering lobe when $L < \lambda \leq 2L$. This is illustrated in figure 4.5.

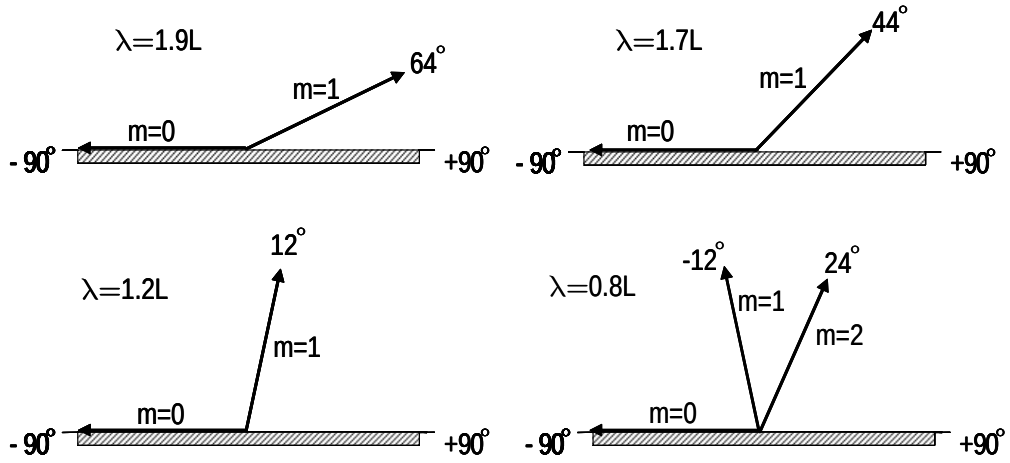

Figure 4.5: *Same illustration as in figure 4.4, but then at an angle of incidence of* $90°$.

Because of the fact that the problem is symmetric, at an angle of incidence of $-90°$ m can only be -1 in equation 4.16 and θ_{-1} will have the same value as $-\theta_1$ at $\psi = 90°$. As can be seen in figures 4.4 and 4.5 the scattering lobes for positive m-values appear at the right side of the specular reflection, whereas the scattering lobes for negative m-values appear at the left side.

Now, assume as an example a scattering surface of which the length of one period is $1\,\mathrm{m}$ and on which a sound wave impinges with a frequency of $2000\,\mathrm{Hz}$. The scattering angles for three different angles of incidence have been calculated, namely $-45°, 0°$ and $15°$. The scattering directions for these angles of incidence are shown in figure 4.6. As mentioned before, the scattering angles at normal incidence are symmetrically distributed around the

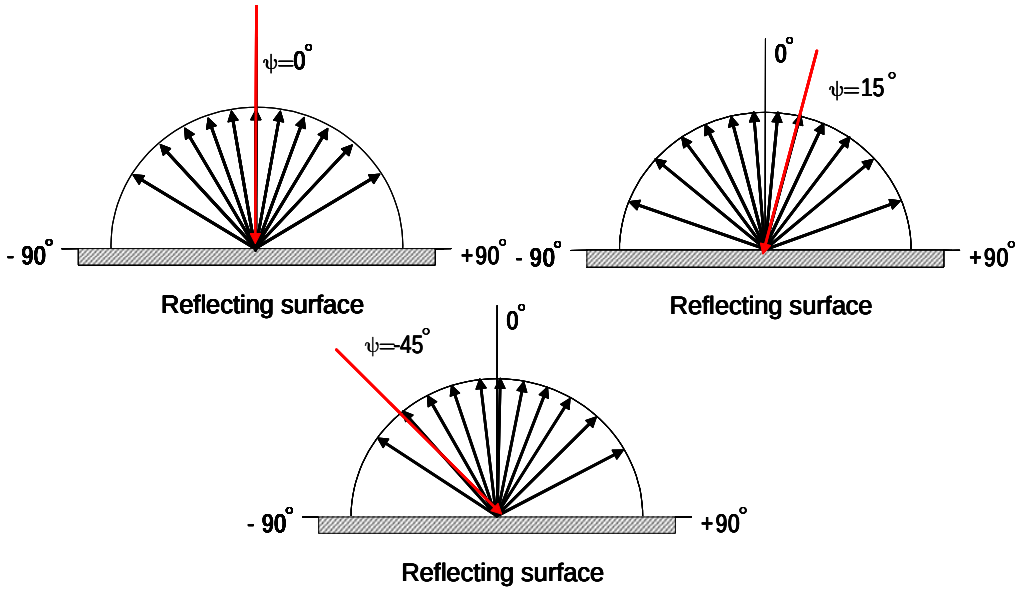

Figure 4.6: *Scattering angles at* 2000 Hz *for three different angles of incidence.*

angle of incidence. However, for oblique angles of incidence this is no longer the case. This is visible in figure 4.6. Also visible is the fact that the angle distance between the different scattering angles is not constant, but grows for larger scattering angles. This is off course a consequence of the $\arcsin$ in equation 4.12.

The reflectivity factor of one well of a diffuser, which is considered a hard scattering object, is defined as

$$R(x,\omega) = R_n = e^{-j\Delta\phi_n} \tag{4.17}$$

with the phase difference in the $n'th$ well given by

$$\Delta\phi_n = 2\pi\frac{2d_n}{\lambda}, \tag{4.18}$$

where d_n is the depth of the $n'th$ well, λ is the wavelength of the impinging sound and R_n is periodic with period N. Now, consider the sequence

$$R'_n = e^{-j2\pi\frac{s_n}{N}} = e^{-j2\pi\frac{n^2 \bmod N}{N}} \tag{4.19}$$

which is also periodic with period N and has the same form as equation 4.17. The discrete spatial Fourier transform of the periodic sequence of R'_n is given by:

$$\widetilde{R}'_{k_{x_m}} = \frac{1}{N}\sum_{n=0}^{N-1} R'_n e^{jk_{x_m}x_n} \tag{4.20}$$

with $k_{x_m} = k\sin\theta_m$ and k the wavenumber. An important property of equation 4.20 is that it has a constant magnitude $\left|\widetilde{R}'_{k_{x_m}}\right|^2 = \frac{1}{N}$. This can be explained as follows [10], [11]: the periodic, normalized (auto)correlation sequence of equation 4.19 is given by:

$$c_\tau = \frac{1}{N}\sum_{n=0}^{N-1} R'_n R'^{*}_{n+\tau} = e^{j2\pi\frac{\tau^2}{N}}\sum_{n=0}^{N-1} e^{j4\pi\frac{n\tau}{N}} \tag{4.21}$$

where the * denotes the conjugate of $R_{n+\tau}$. Now, for any $\tau \neq 0 \pmod N$ the sum vanishes, however for $\tau = 0 \pmod N \Longrightarrow c_0 = 1$. This means that c_τ

can be written as a discrete delta function

$$c_\tau = \delta(\tau). \tag{4.22}$$

An important property of the (auto)correlation sequence is the Wiener-Khinchin Theorem which is given by [12]:

$$c_\tau = DFT^{-1}\{\left|\widetilde{R}'_{k_{x_m}}\right|^2\} \tag{4.23}$$

where DFT^{-1} denotes the inverse discrete (spatial) Fourier transform. From equation 4.23 follows that

$$\left|\widetilde{R}'_{k_{x_m}}\right|^2 = DFT\{c_\tau\} = DFT\{\delta(\tau)\} = \frac{1}{N}. \tag{4.24}$$

From this result and equation 4.20 follows that the sum of $\left|\widetilde{R}'_{k_{x_m}}\right|^2$ for all values of k_{x_m} equals 1 (so, $\sum_{<k_{x_m}>} \left|\widetilde{R}'_{k_{x_m}}\right|^2 = 1$). As mentioned before, R'_n has the same form as R_n. If the magnitude of the discrete spatial Fourier transform of the sequence R_n, $\left|\widetilde{R}_{k_{x_m}}\right|^2$, is also a constant as given by equation 4.24, it means that a wave impinging on the diffuser will be scattered in different directions with *equal* energies. For such a diffuser, the depth d_n in equation 4.18 must be proportional to the quadratic residue sequence s_n. Also, for optimal scattering $0 \leq \Delta\phi_n < 2\pi$ all over the diffuser. By substituting these boundaries into equation 4.18 a range for the depth of the wells is obtained:

$$0 \leq d_n < \frac{\lambda}{2}.$$

As mentioned before the upper boundary $s_{\max} = N - 1$. All these conditions lead to the following equation for d_n:

$$d_n = \frac{\lambda}{2}\frac{s_n}{N} \tag{4.25}$$

for all λ. Later on will be shown that for the design of a QRD the design wavelength $\lambda_{\max}$ is used in equation 4.25. If the depth is given by equation 4.25, then $\left|\widetilde{R}_{k_{x_m}}\right|^2$ will also have a spectrum with a constant magnitude, resulting in a quadratic residue diffuser of which the most important property

is that it scatters energy equally in different directions θ_m, with θ_m given by equation 4.12.

The width of the diffuser elements must be chosen such that the wells can be considered as small wave guides. In wave guides with rigid boundaries, waves have to satisfy the boundary condition that the component of the particle velocity perpendicular to the boundary surface must be zero at the boundaries of the wave guide and as a consequence the waves only propagate in one direction. For this to be true for the diffuser, the width b of the wells must be smaller than half the shortest *apparent* wavelength λ_a (see figure 4.7) for which the diffuser is designed, with λ_a given by:

$$\lambda_a = \frac{\lambda}{\sin\psi}. \tag{4.26}$$

Only then there will be effective diffusion in the range of wavelengths under consideration. This is explained as follows: assume a two-dimensional wave with wavenumber k (with $k = \frac{2\pi}{\lambda}$) that impinges on a well with angle of incidence ψ, see figure 4.7. In this case the wavenumber k consists of two components k_x and k_z, with $k_x = k\sin\psi = \frac{2\pi}{\lambda_a}$ and $k_z = k\cos\psi$. Because of the boundary condition stated above the wave only fits in the well if $k_x = 0, \frac{\pi}{b}, \frac{2\pi}{b}, \frac{3\pi}{b}, ...$ When $k_x \neq 0$ and $k_z = 0$ it is possible for waves to travel in the lateral direction and create standing waves inside the well. When $k_x \neq 0$ and $k_z \neq 0$ the propagation inside the wells will be two-dimensional. This has the following consequences for the width of the wells: the lowest value for the width for which standing waves are able to travel in the lateral direction and two-dimensional propagation is possible, is when $b = \frac{\lambda_a}{2}$ ($k_x = \frac{\pi}{b}$). From this follows that b should be smaller than $\frac{\lambda_a}{2}$. The remaining possibility for k_x is $k_x = 0$, resulting in one-dimensional propagation in the well such as in a wave guide, see figure 4.7. The apparent wavelength can vary from infinitely large at normal incidence to λ at an angle of incidence of $\pm 90°$.

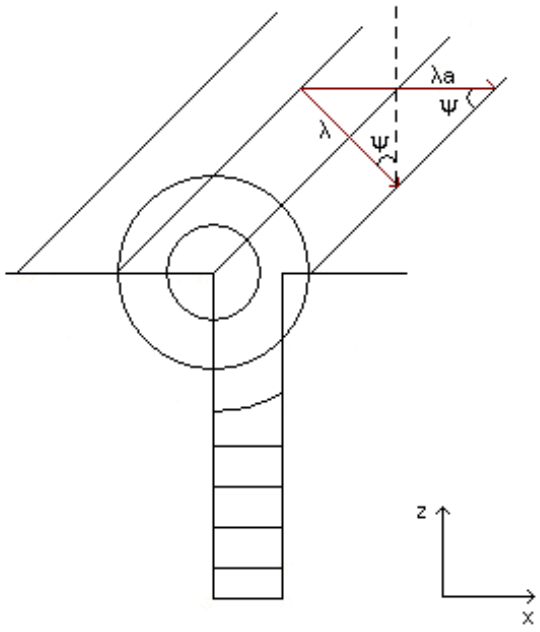

Figure 4.7: *Oblique incidence of a wave with* $\frac{\lambda_a}{2}$ *larger than the width of the well.* λ *is the real wavelength.*

The total width of the QRD is also of importance, because it determines the shape of the grating lobes in the polar distribution. This can be explained as follows: assume a diffuser that consists of an infinite amount of periods. A diffuser that consists of, for example, three periods is the equivalent of the infinitely long diffuser multiplied with a space window that has the length of three periods and a heigth of 1, see figure 4.8.

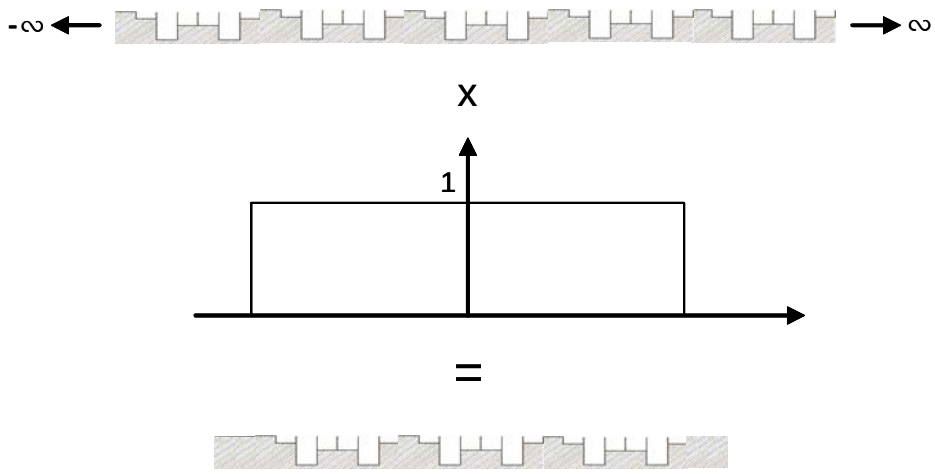

Figure 4.8: *Illustrative picture of the equivalent of a diffuser that consists of three periods.*

Figure 4.8 represents a multiplication in the space domain, which is equivalent to a convolution in the (spatial) Fourier domain [13]. The discrete spatial Fourier transform of a QRD is given by equation 4.20 and consists of pulses in the spatial Fourier domain (for the amount of periods $N_p \rightarrow \infty$) of which the positions are equivalent to the scattering angles ($\theta_m = \arcsin(\frac{m\lambda}{L} - \sin\psi)$). The Fourier transform of the window of figure 4.8 is a sinc function. An important property of such a window is that the width of the window determines the width of the lobes of the sinc function: the broader the window in the space domain, the narrower the lobes of the sinc function in the spatial Fourier domain. So, in the spatial Fourier domain, figure 4.8 respresents the convolution of pulses with a sinc function as illustrated in figure 4.9.

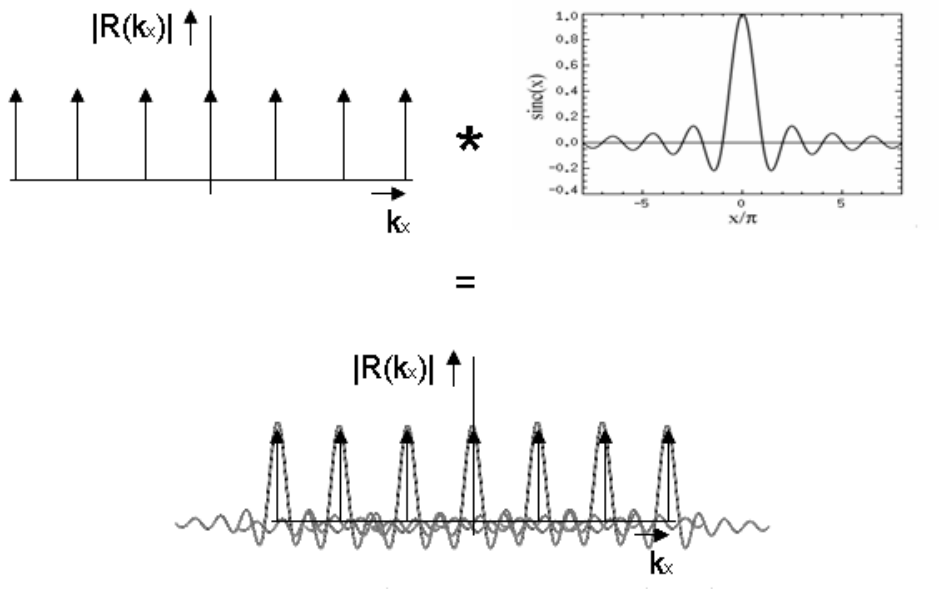

Figure 4.9: *Illustrative scheme of the convolution between a sinc function and the (spatial) Fourier transform of a QRD. The * represents the convolution operator.*

For QRD's this has the consequence that the more periods the diffuser contains (and thus the broader the space window), the narrower the lobes in the polar distribution. An example of this is shown in figure 4.10 ([9], figure 9.6). It is seen that the polar distribution becomes less uniform when

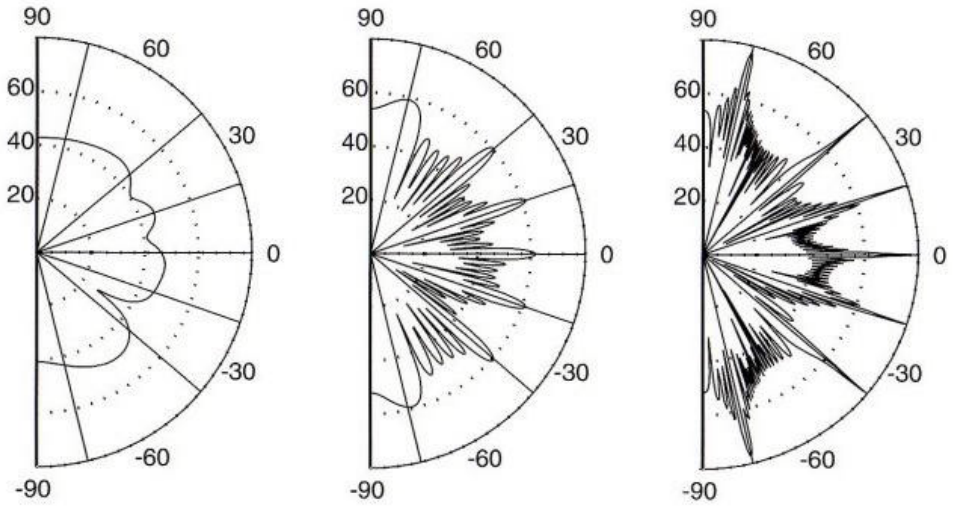

Figure 4.10: *The polar distributions of a QRD with* $N = 7$ *at* $3\,\mathrm{kHz}$ *for (from left to right)* $1, 6$ *and* 50 *periods respectively.*

the diffuser consists of a larger amount of periods and thus when the space window in figure 4.8 becomes wider. This means that a small amount of periods, and equivalently, a narrow space window, is preferable. The extreme situation is when the space window becomes so narrow that it consists of a pulse, leading to a diffuser that consists of a point diffractor which, of course, has a uniform distribution.

4.2.2 Design of a QRD

There are four criteria that can be used for the design of a diffuser. These criteria consist of two low frequency and two upper frequency limits. In practice high frequency sound is easily scattered at irregularities leaving the low frequency limit to be the most decisive: $f_{\min} = f_{design}$. The elementary

relation between the frequency and the wavelength is given by equation 4.27

$$\lambda = \frac{c}{f} \tag{4.27}$$

with λ the wavelength, f the frequency and c the velocity of sound (in this research taken to be $343\frac{\mathrm{m}}{\mathrm{s}}$ at room temperature). According to equation 4.27 the minimum wavelength $\lambda_{\min}$ and maximum wavelength $\lambda_{\max}$ are given by

$$\lambda_{\min} = \frac{c}{f_{\max}} \text{ and } \lambda_{\max} = \frac{c}{f_{\min}} \tag{4.28}$$

with $f_{\min}$ and $f_{\max}$ the minimum and maximum frequency respectively. The four criteria for the design of a diffuser are given below.

Low frequency criteria

1. The first low frequency limit is related to the maximum depth of the wells $d_{\max}$. As mentioned before, the scattering of the quadratic residue diffuser is based on the phase changes $\Delta\phi_n$ that take place in the different wells of which the depths are proportional to s_n. The depth of the wells are given by (equation 4.25):

   $$d_n = \frac{\lambda}{2}\frac{s_n}{N} \tag{4.29}$$

   From equation 4.29 follows that the largest depth $d_{\max}$ is given by:

   $$d_{\max} = \frac{\lambda_{\max}}{2}\frac{s_{\max}}{N} = \frac{\lambda_{\max}}{2}\frac{N-1}{N} \tag{4.30}$$

   By rewriting this equation with the aid of equation 4.28 the first criterion is obtained:

   $$d_{\max} = \frac{c}{2f_{\min}}\frac{N-1}{N} \Longrightarrow f^{(1)}_{\min} = \frac{c}{2d_{\max}}\frac{N-1}{N} \tag{4.31}$$

   As can be seen in equation 4.31, for very low frequencies the diffuser would become very unpractical, because of a very large depth.

2. The second low frequency criterion is that there must be at least two scattering directions: if not, the diffuser would do injustice to its name and in fact would be 'just a reflecting surface'. As was mentioned in subsection $4.2.1$ the scattering angles can be calculated with equation 4.11

where $m = 0, \pm1, \pm2, \pm3...$ etc. Rewriting equation 4.11 using equation 4.27 gives for the frequency

$$f = \frac{mc}{L(\sin\theta_m + \sin\psi)} \tag{4.32}$$

The first order scattering directions occur for $m = \pm1$. For $m = \pm1$ equation 4.32 becomes

$$f = \frac{\pm c}{L(\sin\theta_{\pm1} + \sin\psi)}. \tag{4.33}$$

The boundary values for which there is one scatter direction apart from the specular reflection direction is when $\sin\theta_{\pm1} = \pm1$ (the scattering angles cannot be larger than $\pm90°$). These boundary values determine the minimum frequency at which the diffuser starts working.

$$f_{\min} = \frac{\pm c}{L(\pm1 + \sin\psi)}. \tag{4.34}$$

Considering that $f_{\min}$ should be positive and that $|\sin\psi|_{\max} = \pm1$, leads to (see appendix A):

$$f^{(2)}_{\min} \geq \frac{c}{2L}. \tag{4.35}$$

For normal incidence $(\psi = 0)$ the criterion becomes:

$$f^{(2)}_{\min} \geq \frac{c}{L} \tag{4.36}$$

and there are two scattering angles that are first to appear, namely for $m = +1$ and $m = -1$. This was already visible in figure 4.4. Since inequality 4.36 has a higher boundary value than inequality 4.35 and scattering at normal incidence is preferred to scattering at grazing incidence, it is more strict and thus inequality 4.36 is the second low frequency criterion.

As can be seen in equations 4.31 and 4.36 there are two low frequency criteria of which the first is determined by the depth of the wells and the second by the width ($L = Nb$). Of these two the one with the highest value is the most definite for the working of the diffuser and thus should be chosen to be f_{design}. As a consequence either the depth or the width of the wells is the

most definite design parameter.

Upper frequency criteria

1. The first high frequency limit is to avoid critical frequencies where the diffuser behaves as a flat surface. At this frequency the travelling distance $2d_n$ is a fixed number of the wavelength of the sound wave and the diffuser acts as a flat surface. This situation occurs if the minimum depth (that is not zero) d_1 is equal to half the minimum wavelength, because then $d_n = s_n \frac{\lambda_{\min}}{2}$. As a consequence all critical frequencies are avoided if

$$d_1 < \frac{\lambda_{\min}}{2} = \frac{c}{2f_{\max}} \tag{4.37}$$

   This leads to the second high frequency criterion:

$$f_{\max}^{(1)} < \frac{c}{2d_1} \tag{4.38}$$

2. The second upper frequency limit was already mentioned, namely the fact that the width b of the wells must be smaller than half the shortest apparent wavelength for which the diffuser is designed in order to avoid wave propagation in the lateral direction of the well, so $b < \frac{\lambda_{a_{\min}}}{2}$. The apparent wavelength is given by equation 4.26 and is shortest when $\sin\psi = 1$ and $\lambda = \lambda_{\min}$. This leads to:

$$b < \frac{\lambda_{\min}}{2} \tag{4.39}$$

   With the aid of equation 4.28 this becomes

$$b < \frac{c}{2f_{\max}} \Longrightarrow f_{\max}^{(2)} < \frac{c}{2b} = \frac{cN}{2L} \tag{4.40}$$

As can be seen in equations 4.38 and 4.40 the upper frequency criteria also depend on the width and the depth just as the low frequency criteria. From the design frequency f_{design} follows the most important design parameter (depth or width) and thus which one of the two high frequency criteria is the upper limit. However, one has to check if the remaining upper frequency limit does not have a lower value than the chosen one, because then the effective bandwidth will be smaller. If $f_{\min}^{(1)}$ is the most definite then the corresponding

upper limit is $f^{(1)}_{\max}$. These two limits (equations 4.31 and 4.38) can be used to derive a relationship between the bandwidth, the maximum and minimum depth and the prime number:

$$\frac{f^{(1)}_{\max}}{f^{(1)}_{\min}} < \frac{N d_{\max}}{d_1 \, (N-1)} = N. \tag{4.41}$$

If $f^{(2)}_{\min}$ and $f^{(2)}_{\max}$ determine the effective bandwidth of the diffuser and for $f^{(2)}_{\min}$ the minimum value of equation 4.36 is taken, the relation between the bandwidth and the prime number is given by:

$$\frac{f^{(2)}_{\max}}{f^{(2)}_{\min}} < \frac{N}{2}. \tag{4.42}$$

For oblique angles of incidence

$$\frac{f^{(2)}_{\max}}{f^{(2)}_{\min}} < \frac{N(1+|\sin\psi|)}{2} \tag{4.43}$$

(see appendix A).

Now, assume a diffuser that scatters in the horizontal plane, so the depths of the wells vary in the horizontal direction only. The diffuser has area dimensions of approximately $1 \times 1\,\mathrm{m}$ (common order of magnitude of diffuser dimensions). The prime number for the diffuser is $N = 13$. For this value the sequence of one period of the quadratic residue becomes

$$n^2_{\bmod 13} = 0, 1, 4, 9, 3, 12, 10, 10, 12, 3, 9, 4, 1.$$

An example of what the diffuser according to this sequence should look like is given in figure 4.11.

The diffuser has a width of $1\,\mathrm{m}$ and if the diffuser consists of two periods (as was shown in figure 4.10 a low amount of periods is preferable) the width of one well can be calculated with equation 4.44, where the length L of one period is given by:

$$L = Nb \tag{4.44}$$

By using equation 4.44 the width of the wells becomes $b = \frac{0.5}{13} \approx 0.04\,\mathrm{m}$.

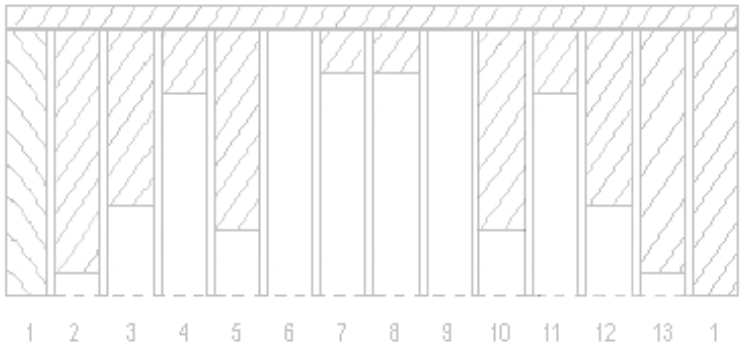

Figure 4.11: *A schematic view from above of one period of a diffuser with prime number $N = 13$, width b and depths d_n.*

The diffuser has a maximum depth of $d_{\max} = 0.34\,\mathrm{m}$. This geometry can be used to calculate the four criteria that are stated above. The four frequency limits (for normal incidence) are given in table 1.

Table 1: *The four frequency criteria for a diffuser with N=13, b=0.04m and dmax=0.34m.*

$f_{\min}^{(1)}$	$500\,\mathrm{Hz}$
$f_{\min}^{(2)}$	$660\,\mathrm{Hz}$
$f_{\max}^{(1)}$	$6500\,\mathrm{Hz}$
$f_{\max}^{(2)}$	$4288\,\mathrm{Hz}$

As can be seen in table 1 there are two different low frequency limits and two different high frequency limits. The low frequency limit for at least two scatter directions is the highest $(660\,\mathrm{Hz})$ which means that for a working diffuser the second low frequency criterion is the most definite. This criterion is dependent on the width of the wells which means that the corresponding high frequency limit is $f_{\max}^{(2)}$. Also visible in the table is that the first high frequency limit $f_{\max}^{(1)}$ has a higher value than $f_{\max}^{(2)}$ and thus does not cause any trouble. So, the effective frequency range for which the diffuser scatters is $660\,\mathrm{Hz} - 4288\,\mathrm{Hz}$. With equation 4.12, the scattering angles can be calculated. These scattering angles are calculated for a number of waves with different frequencies at normal incidence and are shown in table 2.

Table 2: *Scattering angles at normal incidence for different frequencies f*

$f(\mathrm{Hz})$	θ_{-2}	θ_{-1}	θ_0	θ_1	θ_2
500	–	–	$0°$	–	–
660	–	$-88°$	$0°$	$88°$	–
1000	–	-41	$0°$	$41°$	–
1325	$-85°$	$-30°$	$0°$	$30°$	$85°$
1500	$-62°$	$-26°$	$0°$	$26°$	$62°$
2000	7 scattering angles				
3000	9 scattering angles				
3500	11 scattering angles				
4000	13 scattering angles				
4288	13 scattering angles				

In this table it is visible that at $500\,\mathrm{Hz}$ the diffuser does not scatter yet, while at $660\,\mathrm{Hz}$ it does, as was expected. From the fact that equations 4.36 $\left(f^{(2)}_{\min}\right)$ and 4.40 $\left(f^{(2)}_{\max}\right)$ are the most definite criteria, can be concluded that if a different effective frequency range is desired, the diffuser geometry should be altered according to these two criteria. A choice can be made to choose a different prime number or a different well width or both. It is also possible to use equation 4.42 as a rough indication for the prime number or desired bandwidth. However, the other two criteria should be checked to make sure that $f^{(2)}_{\min}$ and $f^{(2)}_{\max}$ are still the most definite criteria.

The angle of incidence also has influence on the effective bandwidth as can be seen in equation 4.43. To illustrate this the scattering angles for an angle of incidence of $\psi = -30°$ has also been calculated and are shown in table 3. As can be seen in the table the diffuser now does scatter at $500\,\mathrm{Hz}$. Also visible is the fact that the scattering is no longer symmetric around the angle of incidence and that the first scattering lobe appears for $m = -1$ as was explained in section 4.2.1 and this section respectively.

As can be seen in tables 2 and 3 the maximum amount of scattering lobes in the effective frequency range is the same as the prime number N. This was also visible in figure 4.10, where the polar distribution of a diffuser with $N = 7$ is shown. This can be explained with the aid of equation 4.13 which states that

$$-1 \leq \frac{m\lambda}{L} - \sin\psi \leq 1. \tag{4.45}$$

Table 3: *Scattering angles at different frequencies f for an angle of incidence of -30 degrees.*

$f(\mathrm{Hz})$	θ_{-4}	θ_{-3}	θ_{-2}	θ_{-1}	θ_0	θ_1
500	–	–	–	$-55°$	$30°$	–
660	–	–	–	$-30°$	$30°$	–
1000	–	–	$-55°$	$-9°$	$30°$	–
1325	–	$-83°$	$-30°$	$0°$	$30°$	$86°$
1500	–	$-55°$	$-22°$	$3°$	$30°$	$70°$
2000	$-55°$	$-29°$	$-9°$	$10°$	$30°$	$56°$
3000	9 scattering angles					
3500	10 scattering angles					
4000	13 scattering angles					
4288	13 scattering angles					

The total number of values integer m can consist of is the same as the number of scattering lobes. For example, if m can be $0, 1$ and 2 at a specific frequency f, there will be three scattering lobes. Rewriting equation 4.45 to an inequality for m leads to

$$\frac{L}{\lambda}\left(\sin\psi - 1\right) \leq m \leq \frac{L}{\lambda}\left(\sin\psi + 1\right) \tag{4.46}$$

From this equation follows that for high frequency sound (and thus small λ) there is a very large amount of scattering lobes which was expected since high frequency sound scatters in different directions very easily. As can be seen in equation 4.46, the number of m values also depends on the width b of the wells ($L = Nb$). So, the width of the wells is not only an important design parameter of the diffuser, it also determines the maximum amount of scattering lobes in the effective frequency range. The total amount of scattering lobes is given by the difference of the boundary values of equation 4.46:

$$\frac{L}{\lambda}\left(\sin\psi + 1\right) - \frac{L}{\lambda}\left(\sin\psi - 1\right) = \frac{2L}{\lambda} = \frac{2Nb}{\lambda} \tag{4.47}$$

The maximum value of equation 4.47 is obtained when $\lambda = \lambda_{\min}$. If the width of the wells given by equation 4.39 is chosen to be $b \approx \frac{\lambda_{\min}}{2}$ this leads to a maximum amount of N scattering lobes. When the difference between $\frac{\lambda}{2}$ and b becomes larger the amount of scattering lobes will become smaller than N.

Chapter 5
Modelling the QRD

5.1 Virtual positioning of the diffuser in the hallway

The diffuser discussed in the previous chapter has been modelled. Before modelling the diffuser the original image of the hallway had to be resampled, because the resolution of this image was too low compared to the geometry of the diffuser. The eventual high resolution resulted in a considerable large processing time and thus the necessity for a fast processor and a computer with sufficient memory available. A horizontal cross section of the resampled image is shown in figure 5.1.

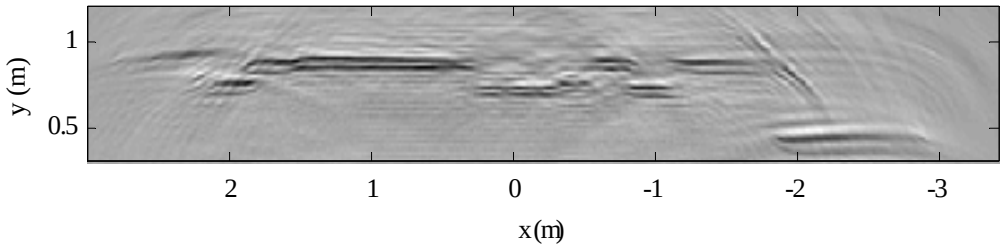

Figure 5.1: *Resampled image of the wall at height* $z = 1.28\,\mathrm{m}$.

The diffuser was placed between the two columns in the hallway and is indicated by the red rectangle in figure 5.2. The coordinates of the diffuser are $z = 0.5\,\mathrm{m}$ to $z = 1.54\,\mathrm{m}$ and $x = -0.01\,\mathrm{m}$ to $x = 1.03\,\mathrm{m}$. Note that the objects displayed in the figure are not on scale in order to emphasize the objects and their positions in the hallway.

As can be seen in figure 5.2 the fuse box is partly being overlapped by the diffuser. So, a piece of a wall and a piece of fuse box were replaced by the

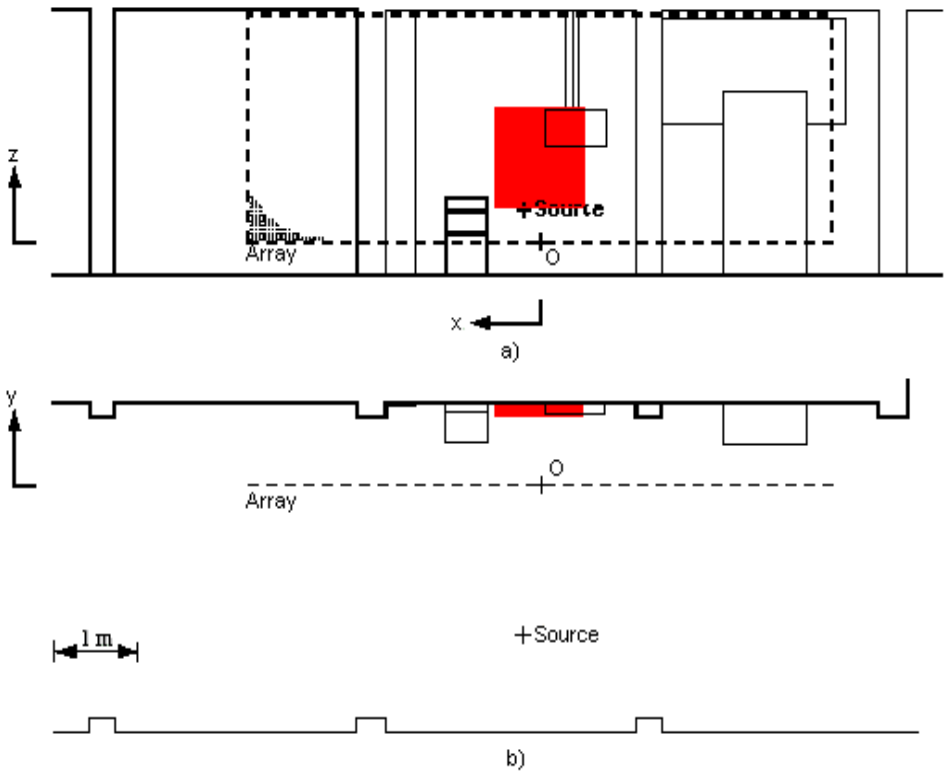

Figure 5.2: *Schematic representation of the position where the diffuser was placed.*

diffuser, whereas the remaining part of the fuse box was replaced by a piece of wall. At this position other objects are at a considerable distance from the diffuser.

Because of the fact that the image resolution is determined by the used source wavelet with which the image is modelled, an image point of the wall of the original image has been used to model the QRD. An image point represents the convolution between the geometry and the source wavelet. The image point of a piece of wall (wallpoint) that is used for modelling the QRD is indicated by the arrows in figure 5.3 where a horizontal slice is shown at height $z = 1.08\,\mathrm{m}$. A cross section of the horizontal slice at the position of the wallpoint indicated by the arrows, is shown in figure 5.4.

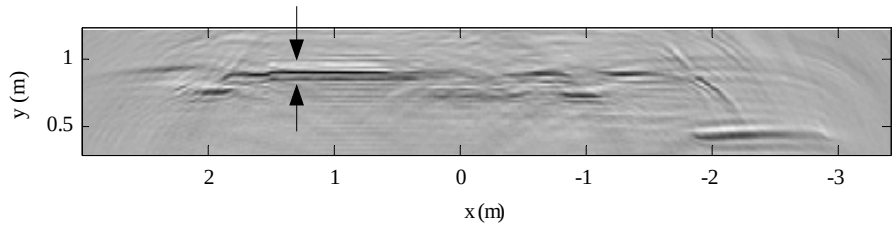

Figure 5.3: *The two arrows indicate the image point that is used for the modelling of the diffuser.*

As was shown in subsection 4.2.2 the width of the wells is taken to be $0.04\,\mathrm{m}$. For the development of the diffuser a piece of wall with this width has been made. The diffuser is then made by copying this wallpiece at the different depth positions according to equations 4.29 and 4.30. The result is shown in figure 5.5. In this figure each piece of wall is indicated by a black rectangle and consists of three copied wallpoints. The analogy between the grayscaled bands in figure 5.5 and the wallpoint in figure 5.4 is shown in figure 5.6.

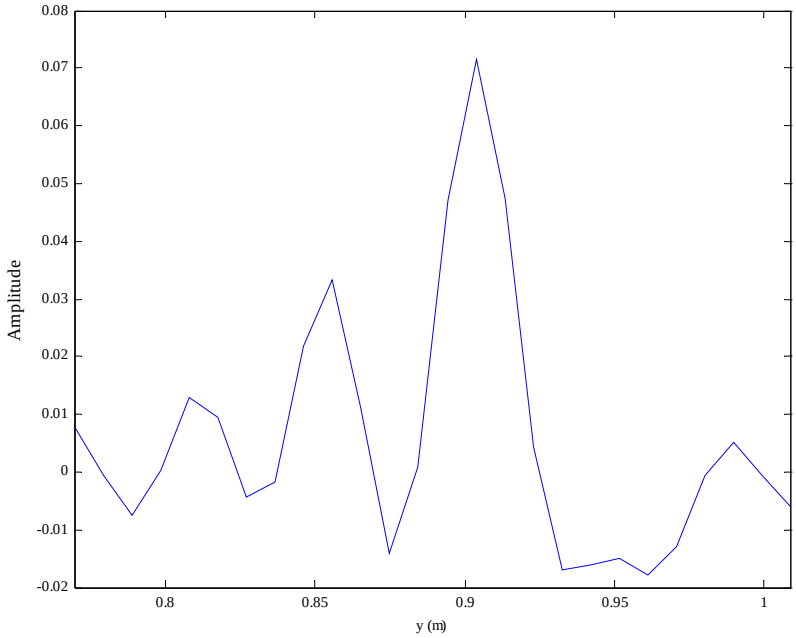

Figure 5.4: *Image point of the wall indicated by the arrows in figure 5.3.*

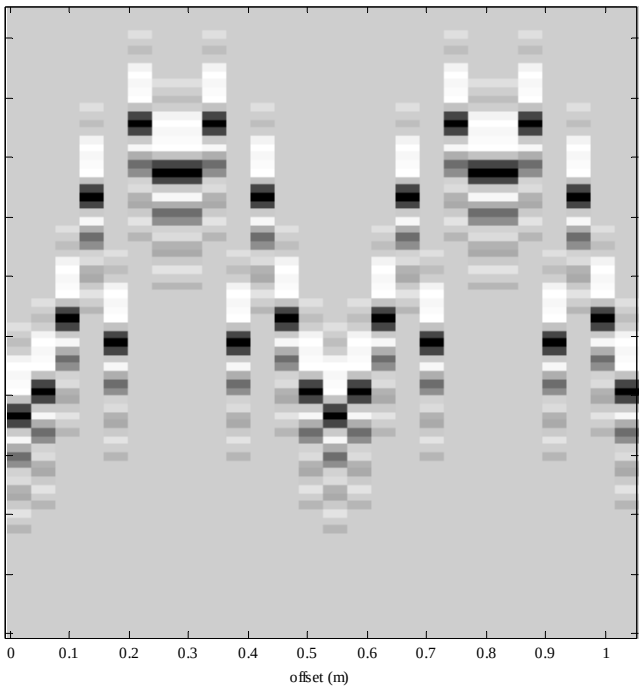

Figure 5.5: *Model of the diffuser.*

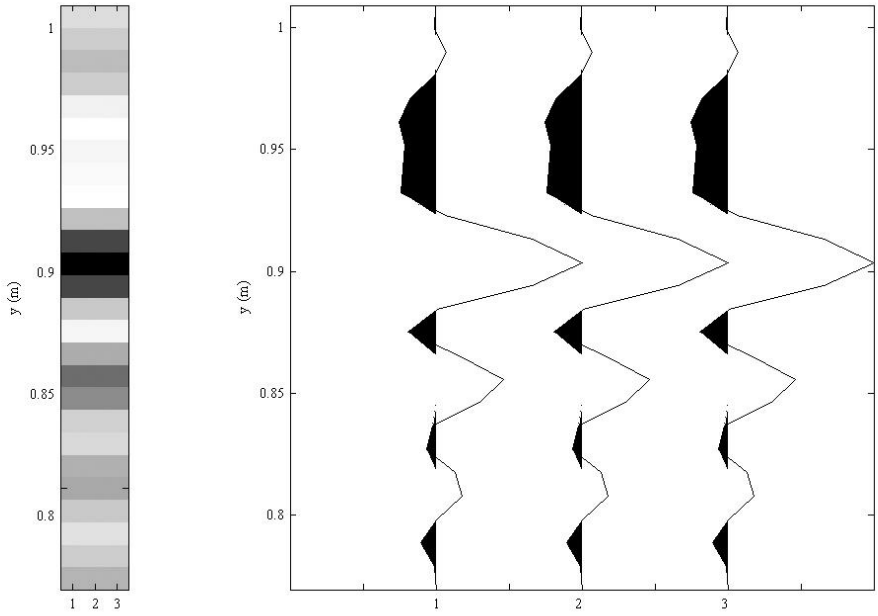

Figure 5.6: *On the left one wallpiece is displayed and on the right the analogy in terms of the wallpoint displayed in figure 5.4.*

After the modelling the diffuser is virtually placed in the hallway by demigrating a piece of the wall, the fuse box and the diffuser and migrating the diffuser to their positions. The impulse response of the original hallway is displayed in figure 5.7 where the reflections of the fuse box and the piece of wall are indicated by a black box. The impulse response of the hall with the diffuser is shown in figure 5.8.

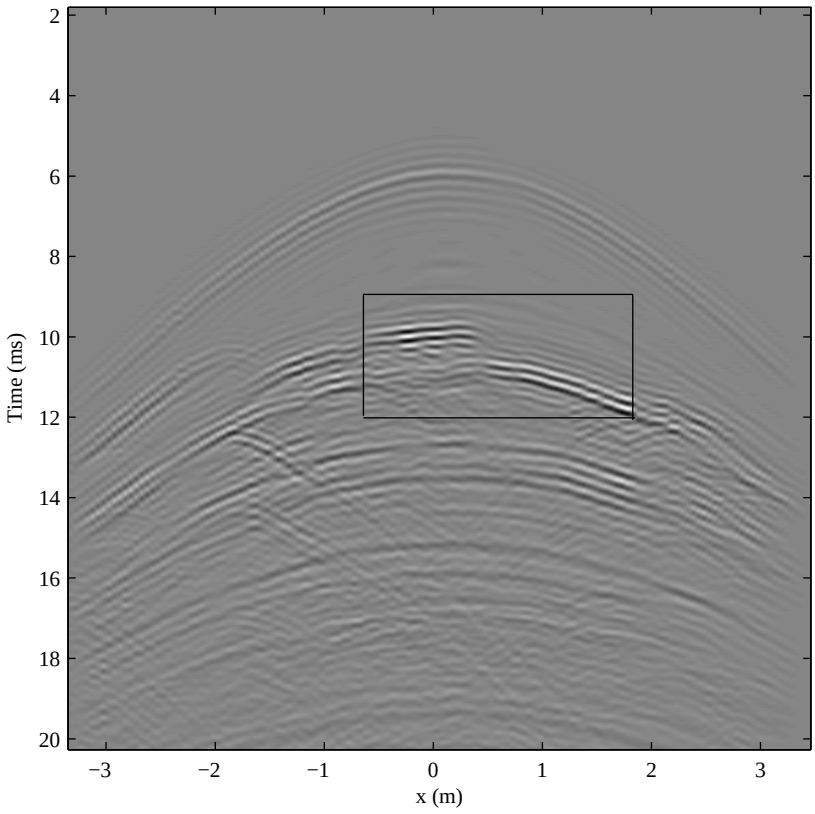

Figure 5.7: *Impulse response of the original hallway.*

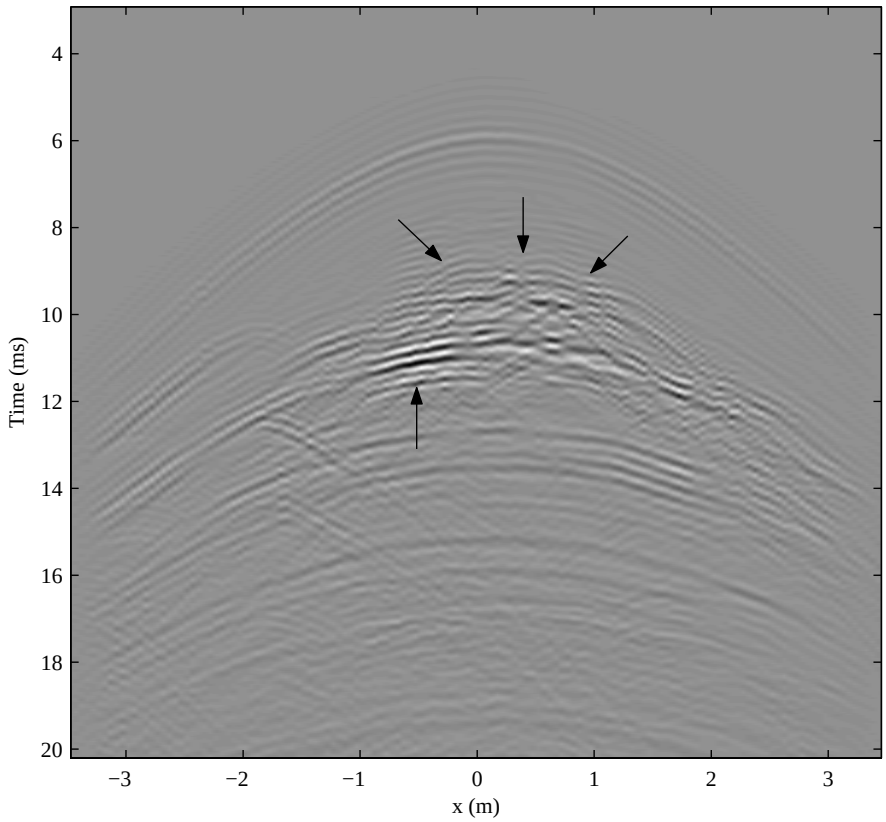

Figure 5.8: *The impulse response of the hall with the diffuser at a height of* $z = 1.5\,\mathrm{m}$.

The reflections of the diffuser are clearly visible between $x = -0.2\,\mathrm{m}$ and $x = 1.1\,\mathrm{m}$ and are indicated by the three arrows pointing downwards. The piece of wall placed on the position of the fuse box is also visible and indicated by the arrow pointing upwards. The difference with the impulse responses at the same positions in figure 5.7 (indicated by the black box) is clearly visible.

As mentioned before the contribution of a diffuser to the perception of sound is that it gives the listener a feeling of spaciousness. This is a consequence of the fact that the diffuser creates reflections that lead to binaural dissimilarity, which was explained in section 4.1. Now consider figure 5.9, where again the impulse response of the hallway with a flat wall at

the position of the fuse box is displayed (see section 3.3).

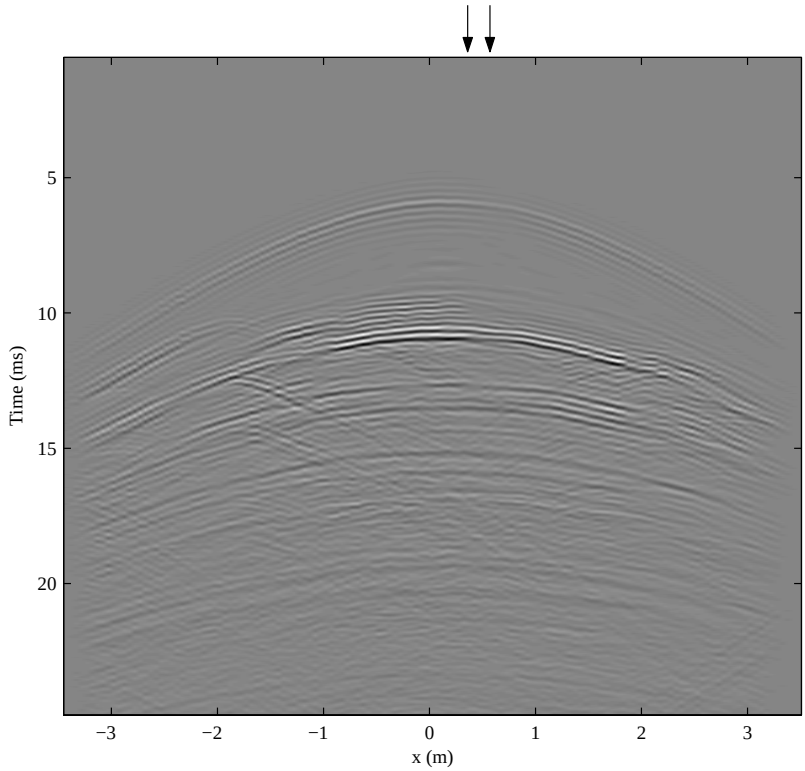

Figure 5.9: *The impulse response of the hallway with a flat wall between the columns at a height of* $z = 1.5\,\mathrm{m}$.

The arrows displayed in figure 5.9 are about $20\,\mathrm{cm}$ apart, approximately the same distance as the distance between the ears on a (human) head. By comparing the impulse responses of the positions indicated by the arrows to the impulse responses at the same positions in the case where the diffuser is placed between the columns in the hall, it can be seen if the placement of the diffuser indeed leads to a higher binaural dissimilarity. The impulse responses of left and right ear are displayed in figure 5.10.

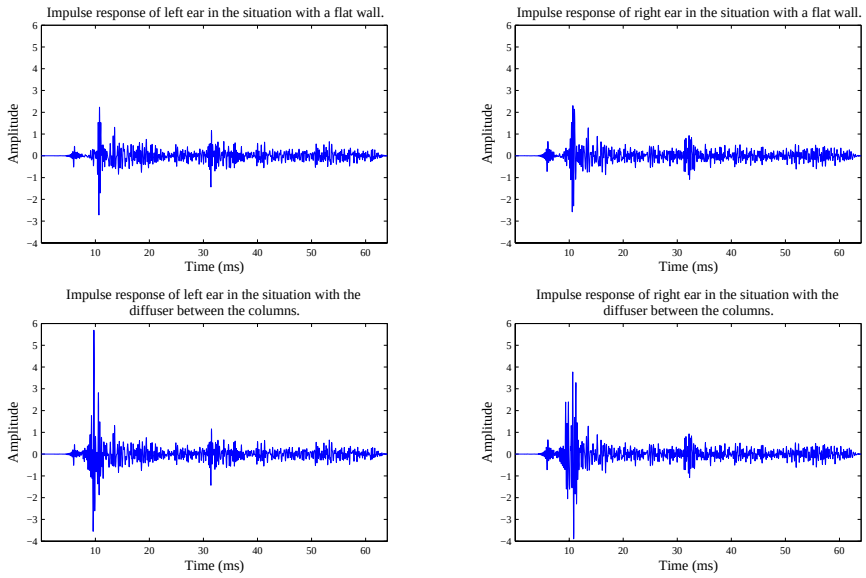

Figure 5.10: *Impulse responses of left and right ear in the cases with and without the diffuser present in the hallway.*

When the impulse responses of left and right ear are compared in figure 5.10 it is visible that in the case *with* the diffuser a (large) difference in amplitude is visible between the signals arriving at left and right ear. Also visible is the difference in arrival times at left and right ear of the reflections with the largest amplitudes. To quantify the difference between the signals the (normalized) cross correlation of the impulse responses arriving at the left and the right ear shown in figure 5.10 has been calculated. In the situation with the diffuser between the columns the cross correlation has a value of 0.39 and in the situation with the flat wall the cross correlation has a value of 0.52. A value of 1 would indicate that both signals are 100% correlated. The values for the cross correlation indicate a higher binaural dissimilarity in the hallway with the diffuser. If this difference is really audible was tested by performing listening tests, which are discussed in the next chapter.

In figure 5.8, where the impulse response of the hallway with diffuser was shown, the form of the diffuser is not very clear, because we are looking

at travel times. So to verify that the demigration was successful, horizontal slices made after re-imaging are shown in figure 5.11.

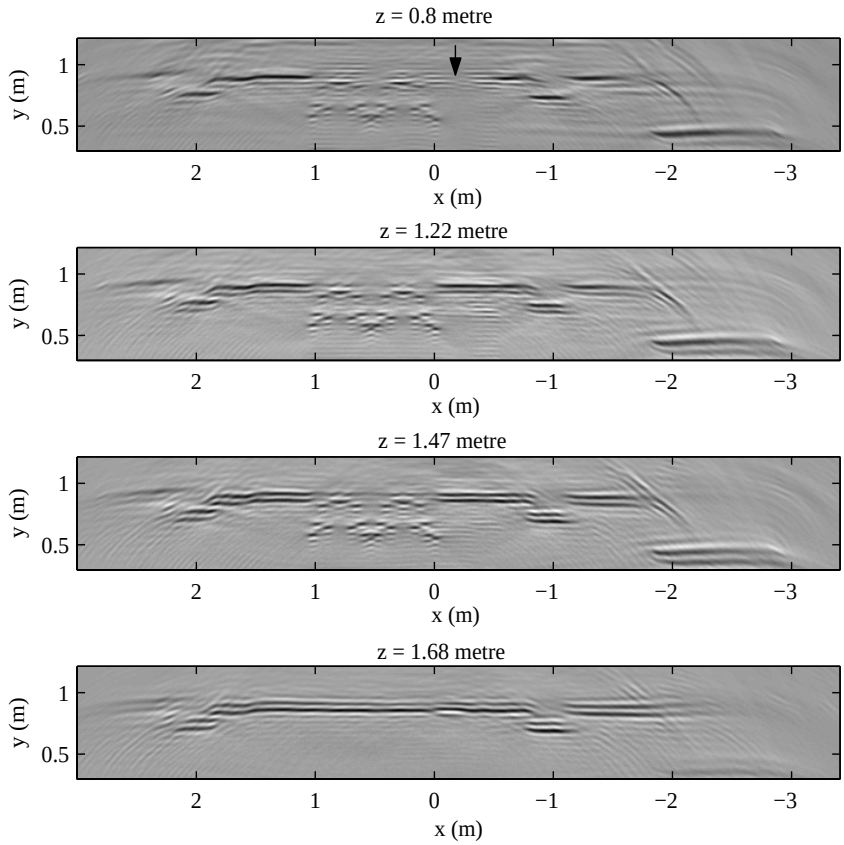

Figure 5.11: *Horizontal slices of the wall with diffuser at different heights.*

In the figure the periodicity of the diffuser is clearly visible and similar to that in figure 5.5. However, at height $z = 0.8\,\mathrm{m}$ on the right side of the diffuser (indicated by the arrow) it seems that there is a hole in the wall. But this is not a real hole. This position is right below the position of the fuse box when it was still there. It can be seen as an acoustic shadow that was already there in the original image on the positions above and below the fuse box and above the closet. This is shown in the images of the original hallway in figure 5.12.

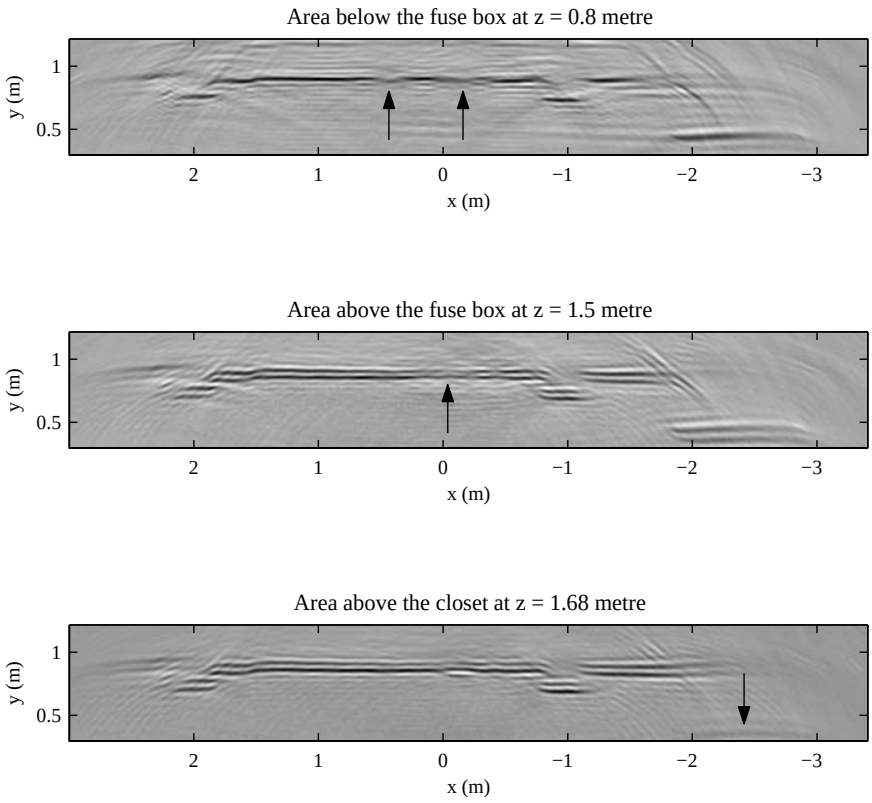

Figure 5.12: *Horizontal slices of the original image of the hallway below and above fuse box and above closet. The arrows indicate the 'holes'.*

In the slices of the fuse box at the positions indicated by the arrows, the wall is not clearly visible; it is a bit blurred and has the appearance of a hole. In the slice of the closet it also appears that there is nothing present, but when looking at a higher position the wall becomes visible. So there seems to be a transition area. In this area there is less acoustic energy impinging on the wall and thus less acoustic energy from this piece of wall reaches the array. It can be compared with light rays falling on an object. Behind the object there will be a shadow as a consequence of light rays not reaching that area, because the object itself is in the path of the rays. A similar effect occurs with sound waves. In figure 5.13 the three-dimensional image of the hallway with the diffuser is displayed. The diffuser is clearly visible bewteen the two columns in the hallway.

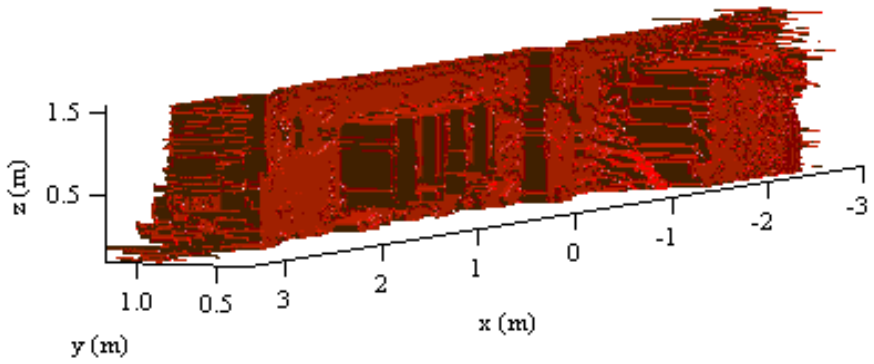

Figure 5.13: *Three-dimensional image of the hallway with diffuser.*

5.2 The influence of the diffuser on the environment in terms of energy distributions

According to the images in the previous section, the placement of the diffuser in the hallway seems successful. An other way to look at the contribution of the diffuser to the reflected sound is by calculating the energy difference between the hall with diffuser and the hall with a flat wall between the

columns.

The energy distribution is calculated in two different ways. In figure 5.14 the energy distribution of only the diffuser in the (x, z)-plane is shown and figure 5.15 shows the energy difference between hallway with diffuser and hallway with a flat wall in the same area.

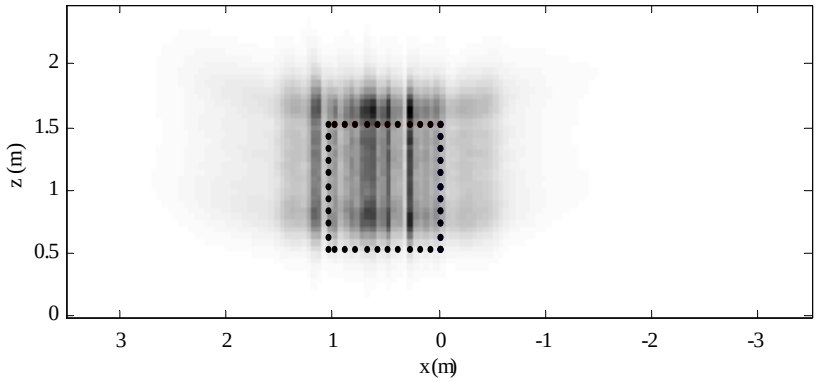

Figure 5.14: *Energy distribution of the demigrated diffuser.*

The diffuser is placed between $x = -0.01\,\mathrm{m}$ and $x = 1.03\,\mathrm{m}$ and in the figure an alternating pattern of high and low energy densities is visible as was expected. In figure 5.14 it is seen that for a certain area outside the boundaries (on the left and right) of the diffuser the energy distribution is not zero and also a bit alternating. This is explained by the fact that the diffuser was modelled to scatter in the horizontal plane. There is also an energy density visible above the diffuser (above $z = 1.5\,\mathrm{m}$). This is probably a result of the fact that the source was placed at a heigth of $z = 0.37\,\mathrm{m}$, which means that the sound impinging on the diffuser comes from below.

In figure 5.15 the horizontal energy distribution outside the boundaries of the diffuser is also visible as well as the alternating pattern of high and low energy densities. However, the distribution is somewhat different. This can be understood by considering figure 5.14 as an energy difference between the energy distribution of the diffuser and zero, while figure 5.15 displays the

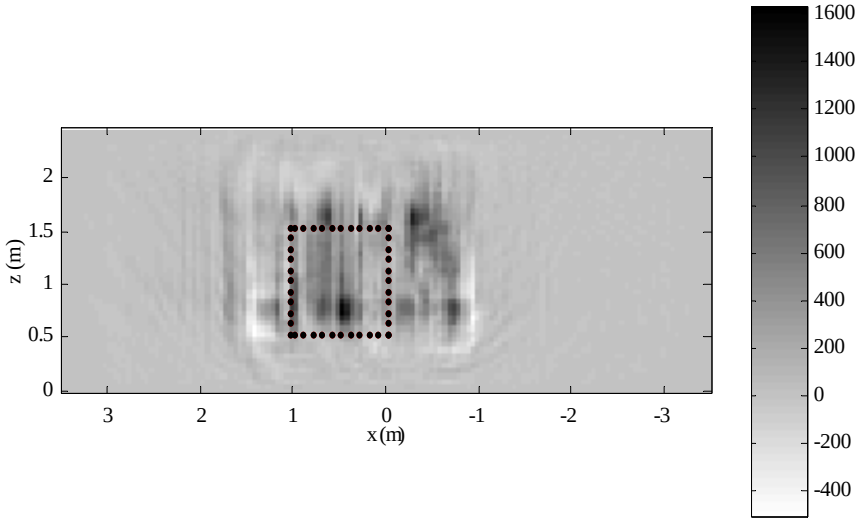

Figure 5.15: *Energy distribution of hallway with diffuser minus hallway with a flat wall.*

energy difference between hallway with diffuser and hallway without diffuser of which the latter is now not zero. It is important to notice that in figure 5.15 there are some white areas that correspond to a negative energy difference while the gray area outside the reach of the diffuser corresponds to zero; the colorbar is added to clarify this. This means that at those positions the energy in the hall with a flat wall is higher than the energy in the hall with the diffuser.

Chapter 6
Listening tests

The influence of adding the diffuser in the hallway is evaluated perceptually by performing listening tests with samples of the hallway with and without the diffuser. Two test signals have been used, a speech signal and a noise signal. Speech is a transient sound and therefore the reflection will either add to the loudness or be perceived as a distinctive echo, dependent on the delay time. Noise, on the other hand, is a continuous sound (in terms of loudness) and therefore the reflection will cause spectral coloration.

6.1 The experiment

The test was performed binaurally with closed headphones and two impulse responses selected at the approximate ear separation distance. The impulse responses were convolved with two monophonic signals. One was a noise sample of two seconds shaped by the spectrum of male speech, the other a four seconds long female speech sample.

The test was a triple stimulus AXB listening test where X was always the sample with the diffuser. This was unknown by the subjects. Either A or B was the sample with the diffuser and the subjects had to choose whether A or B was equivalent to X. The subjects were allowed to listen to a number of randomly selected sets for training purpose before the actual test was started. During the test there was a possibility to repeat the sets as many times as was necessary.

There were 19 listening positions and the signals were fed to the subjects as if they were facing the wall. Using the coordinates of the listening positions, the shortest distance to the reflecting diffuser has been calculated and is $0.54\,\mathrm{m}$. The positions were chosen on two different heights, $0.75\,\mathrm{m}$ and $1.5\,\mathrm{m}$, and a variety of lateral positions. The listening positions were chosen in such a way that the energy ratios of the samples of the hallway with

a flat wall and the hallway with the diffuser were distributed between 0.57 and 1.06 (relatively large energy difference to hardly any difference at all). The listening positions are indicated in figure 6.1.

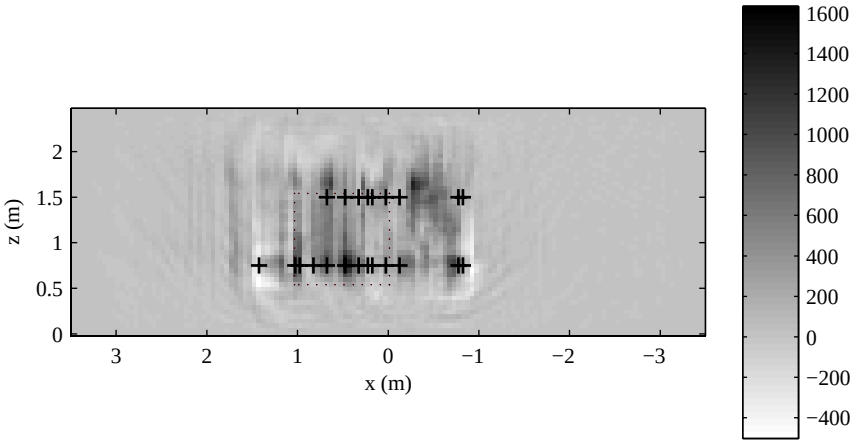

Figure 6.1: *Chosen listening positions indicated with crosses at heigths* $z = 0.75\,\mathrm{m}$ *and* $z = 1.5\,\mathrm{m}$. *The dotted rectangle marks the position of the diffuser.*

18 subjects participated in the test. Some are active players of a musical instrument, others have some experience with listening tests and some of the subjects had no experience with listening tests at all.

6.2 Results

The results of the listening test are shown in figure 6.2 and are displayed as the fraction of correct answers versus the energy ratio of the samples. The threshold lies at 0.75, because statistically there is a 50 percent chance to guess the correct answer.

In the figure it can be seen that in case of the noise signal the values lie close to unity, except at an energy ratio of 0.92. In the case of the speech signal there is also a decrease near 0.9 and near 0.65 which is rather strange, because there is a large energy difference between the samples and the

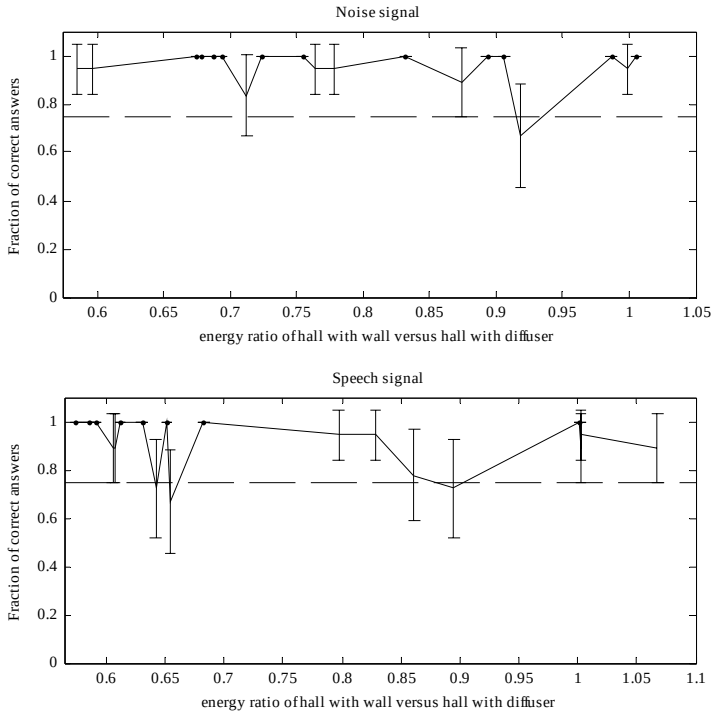

Figure 6.2: *Results of the listening test expressed as mean between the subjects with* 95% *confidence bounds.*

difference should be heard. But the confidence bounds are so large that the overall conclusion is that the differences are audible, even at an energy ratio of approximately 1, while the expectation was that at this ratio it would be more difficult to hear the difference. The reactions after the test were that the subjects had more difficulty with the speech signal than with the noise signal which is confirmed by the results in figure 6.2.

A possible cause of this outcome is that the energy ratio of the samples is not an ideal measure for the amount of wrong answers. It is not an ideal measure, because the energy ratio can be the same for a number of samples while the impulse responses arriving at left and right ear are very different for those samples. Because of this difference there has been a study of the relation between the amount of wrong answers and the energy ratio of the signals arriving at the left and right ear. The result was that there is no correlation

between those two, see figure 6.3.

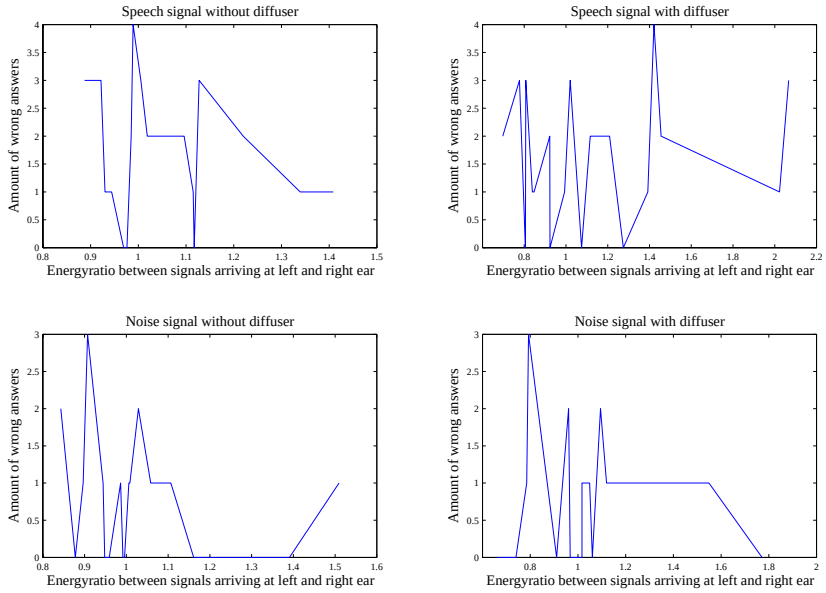

Figure 6.3: *Relation between the amount of wrong answers and the energy ratio of the signals arriving at left and right ear for the different sound samples.*

To check for another relation, the cross correlation between left and right ear in the case of hallway with and hallway without diffuser has been analyzed in relation to the amount of wrong answers. This has been done, because of the fact that if the signals arriving at the left and the right ear are as uncorrelated as possible, the listener experiences a feeling of spaciousness (binaural dissimilarity, see section 4.1). $crem$ is the cross correlation between left and right ear in the case of hallway without the diffuser and $cori$ is the cross correlation between left and right ear in the case of the hallway with the diffuser; the difference is given by $c_{diff} = crem - cori$. If c_{diff} has a high value, the listener is supposed to experience more spaciousness in the hall with the diffuser. If this difference is audible the amount of wrong answers should be low at a high value of c_{diff}. The result is shown in figure 6.4.

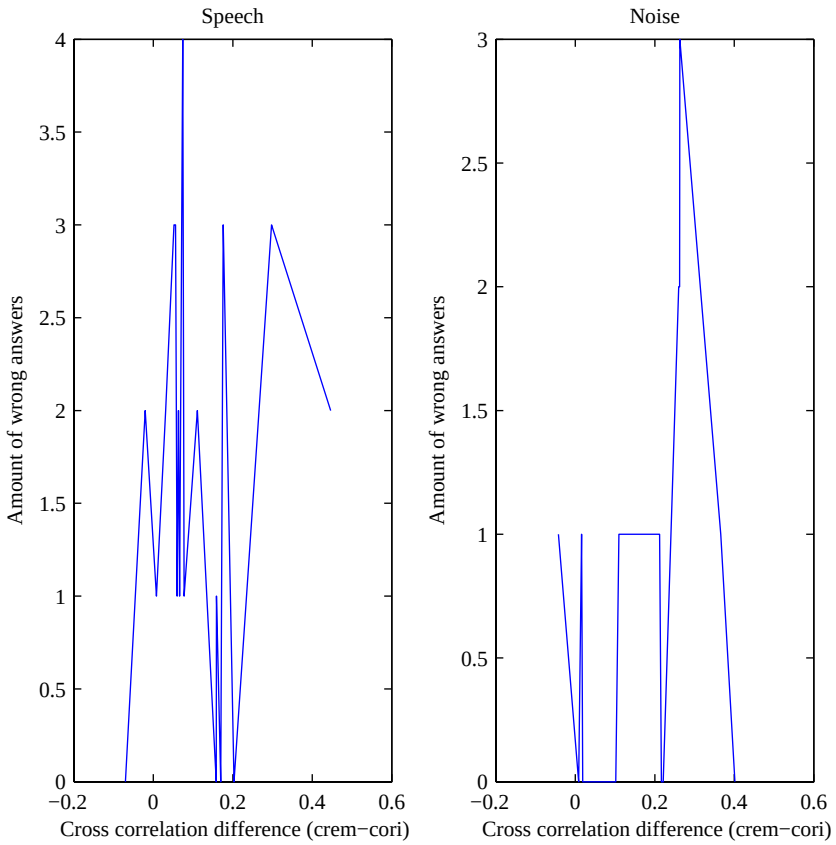

Figure 6.4: *The relation between the amount of wrong answers and the difference in cross correlation of the ears for the hallway with the diffuser and the hallway without the diffuser.*

For the speech signal the amount of wrong answers varies between 0 and 4; for the noise signal the amount of wrong answers is either 0 or 1, except for a peak value of 3 at one of the highest cross correlation differences. The peak value was expected to be near a cross correlation difference of 0 as with the speech signal, because then there is no difference in binaural dissimilarity. From the figure can be seen that the distribution of wrong answers is very random, apparently there is no clear relation between the amount of wrong answers and the difference between both cross correlations and thus, also binaural dissimilarity is not a good measure for the amount of wrong answers.

6.3 Comparison with earlier results

In Kuster's research [1] the fuse box and the closet were removed leaving holes in the hallway. This removal results in the fact that sound energy is able to escape through the holes and is not reflected towards the array. Listening tests have been performed comparing the original hallway with the hallway where the fuse box and closet were removed. At the listening positions in front of the closet the difference between hallway with closet and hallway without closet was well detected by the listeners. However, for the fuse box this proved to be much more difficult.

As mentioned in the previous section, listeners had little trouble detecting the difference between hallway with and hallway without the diffuser. As was the case with the closet. The fact that the difference was harder to detect in the case of the fuse box can be explained by the fact that the fuse box is a considerably smaller object than either closet or diffuser and therefore produces less reflections than the other two objects. Because there are less reflections from the fuse box and thus less reflection energy the difference between fuse box and no fuse box will be harder to hear.

For a more quantitative comparison of the results in this research with Kuster's results, the amount of wrong answers at similar positions is compared. There was only one position in Kuster's listening test that was similar to a position in the test in this research. To obtain more

samples a maximum distance of $5\,\mathrm{cm}$ (one microphone position further) between Kuster's samples and samples used in this research was chosen for comparison. For this maximum distance there were 4 'corresponding' sample positions (including the position that was similar). For both the noise and the speech signal the amount of wrong answers was (much) larger in Kuster's research as can be seen in table 4.

Table 4: *Comparison of the amount of wrong answers given for both signals.*

Sample position (x, z)		Noise		Speech	
This research	Kuster's research	This research	Kuster	This research	Kuster
$(0.175, 1.5)$	$(0.175, 1.5)$	0	2	0	4
$(0.175, 1.5)$	$(0.225, 1.5)$	0	3	0	3
$(0.025, 1.5)$	$(0.075, 1.5)$	1	2	0	4
$(0.325, 1.5)$	$(0.375, 1.5)$	1	7	1	6

In the case of the diffuser the difference was also audible at an energy ratio of approximately 1, contrarily to Kuster's results. One possible explanation was already given in the previous section. The different results can also be a consequence of the different contribution of a diffuser to the perception of sound as explained in chapter 4.

Chapter 7
The diffusion and scattering coefficients

In this research calculations of the energy distribution of the hallway with and without diffuser and listening tests have been used to quantify the performance of the modelled diffuser. In this chapter two other methods to quantify and/or predict the performance of a diffuser are being introduced, which are at the moment being studied in a follow up research. In previous studies the performance of (physical) diffusers has been quantified by measuring their polar responses. Different methods have been used to measure the reflections, for example measurements where the microphones are arranged in a semicircle in front of the diffuser or measurements where a microphone is placed on a hemisphere and the diffuser is placed in the centre of the base. If this (measured) data can be represented by a single value that is a measure for the diffuser performance, it would be easier to work with. More information about the contents of this chapter can be found in [9].

Two new coefficients have been introduced to quantify the performance of a diffuser [9]: the diffusion coefficient and the scattering coefficient, defined as follows:

- The diffusion coefficient measures the diffusibility of a surface by measuring the similarity between the scattered polar response and a uniform distribution.
- The scattering coefficient is a measure of the amount of sound (energy) scaterred away from a particular direction or distribution (for example, the specular direction).

7.1 The diffusion coefficient

For the definition of the diffusion coefficient the autocorrelation function is

used, because it seemed to be the most favourable of the available statistical operations with respect to losing information during data reduction [9]. The autocorrelation is used to measure the scattered energy's spatial similarity between different receiver angles. So, if a surface scatters sound uniformly to all receivers the spatial autocorrelation function will have high values. On the other hand, a surface of which the scattered energy is concentrated in one specific direction will produce low values. It is called the autocorrelation diffusion coefficient, because the autocorrelation function is used *spatially* to measure the similarity between different sections of polar responses. The autocorrelation diffusion coefficient is given by [14], [15]:

$$d_\psi = \frac{\left(\sum_{i=1}^{n} E_i\right)^2}{n\sum_{i=1}^{n} E_i^2} \ , \tag{7.1}$$

where E_i is the squared pressure at microphone i, n is the number of receivers in the polar response and ψ is the angle of incidence. As an example, imagine an array of five receivers in the polar response. In the fully non-diffusive case that the reflections of a surface arrive at one receiver only, thus for example $E_4 = 1$ and $E_1 = E_2 = E_3 = E_5 = 0$, the diffusion coefficient $d_\psi = \frac{1}{5} = \frac{1}{n}$, the minimum value. In the fully diffusive case that the reflections arrive equally strong at every receiver and thus $E_1 = E_2 = ... = E_5 = 1$, the diffusion coefficient $d_\psi = \frac{25}{25} = 1$, the maximum value. Equation 7.1 can be rewritten to:

$$d_\psi = \frac{\left(\sum_{i=1}^{n} 10^{\frac{L_i}{10}}\right)^2}{n\sum_{i=1}^{n}\left(10^{\frac{L_i}{10}}\right)^2} \ , \tag{7.2}$$

where L_i are a set of sound pressure levels in decibels. Equation 7.2 is bounded between $\frac{1}{n}$ and 1 as was shown in the example given above. By a

simple scaling the boundary values can be transformed to 0 and 1:

$$d_\psi = \frac{\left(\sum_{i=1}^{n} 10^{\frac{L_i}{10}}\right)^2 - \sum_{i=1}^{n}\left(10^{\frac{L_i}{10}}\right)^2}{(n-1)\sum_{i=1}^{n}\left(10^{\frac{L_i}{10}}\right)^2}. \tag{7.3}$$

Using the same example given above, the non-diffusive case now gives a diffusion coefficient of $d_\psi = 0$ and for the fully diffusive case $d_\psi = 1$. The diffusion coefficient can be calculated with the demigration routine used in this research by, for example, demigrating the wallpoints to a circular array instead of a planar array. This way a polar response is obtained. Next, the sound pressure level in decibels for each microphone position can be calculated and the diffusion coefficient is obtained with equation 7.3.

7.2 The scattering coefficient

The scattering coefficient separates the reflected sound energy into specular and scattered components as illustrated in figure 7.1. The specular, scattered

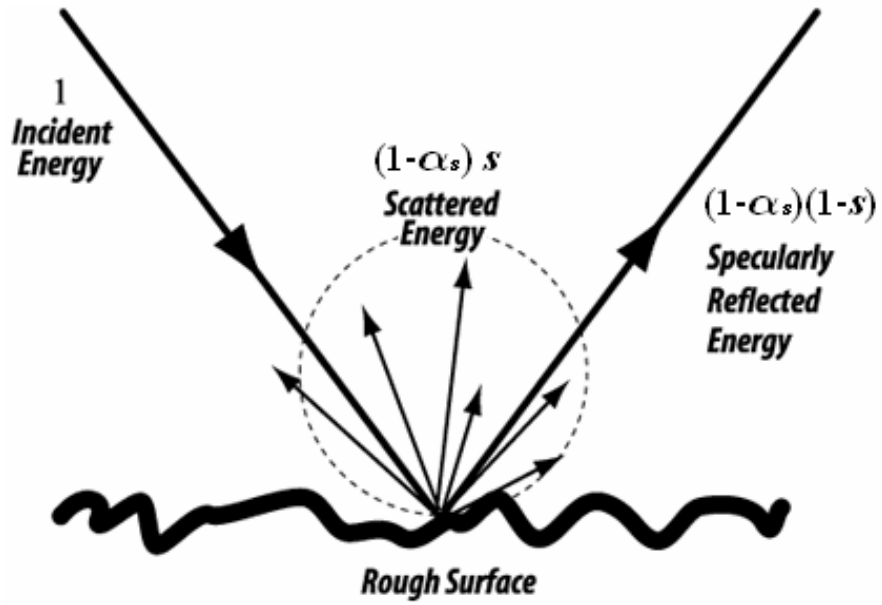

Figure 7.1: *Scattering from a rough surface.*

and total energy of the reflections are given by.

$$E_{spec} = (1-\alpha)(1-s) \equiv (1-\alpha_{spec}) \tag{7.4}$$

$$E_{scat} = (1-\alpha)s \tag{7.5}$$

$$E_{total} = E_{spec} + E_{scat} = 1-\alpha, \tag{7.6}$$

with $s = \frac{E_{scat}}{E_{total}}$. E_{spec} is the specularly reflected energy, E_{scat} the scattered energy, E_{total} is the total reflected energy, s the scattering coefficient, α the known absorption coefficient (which can be obtained using measurements of the reverberation time [9]) and α_{spec} is the apparent specular absorption coefficient. The apparent specular absorption coefficient represents all the energy that is not reflected to the specular reflection direction. α_{spec} can be determined by measuring the specularly reflected energy. This is done by placing the scattering surface on a turntable and measuring the reflections while the table is rotating [9]; the set up is shown in figure 7.2. The initial parts of the reflections are highly correlated, forming the specular components which remain unaltered as the sample is rotated. The later parts consist of the scattered components. This can be explained as follows: assume a set up as on the left hand in figure 7.3,where the specular reflection of a scattering surface is shown. The pathlength $SR1M$ is the same as the pathlength $SR1M'$ from the source via the specular reflection point to the projection of the microphone (M') on the other side of the reflecting surface. The same holds for other reflection points on the scattering surface, see the right hand in figure 7.3. The triangular inequality [16] states that for a triangle as given in figure 7.4:

$$|AB| < |AP| + |BP| \tag{7.7}$$

and only if P lies on the line between points A and B

$$|AB| = |AP| + |BP|\,. \tag{7.8}$$

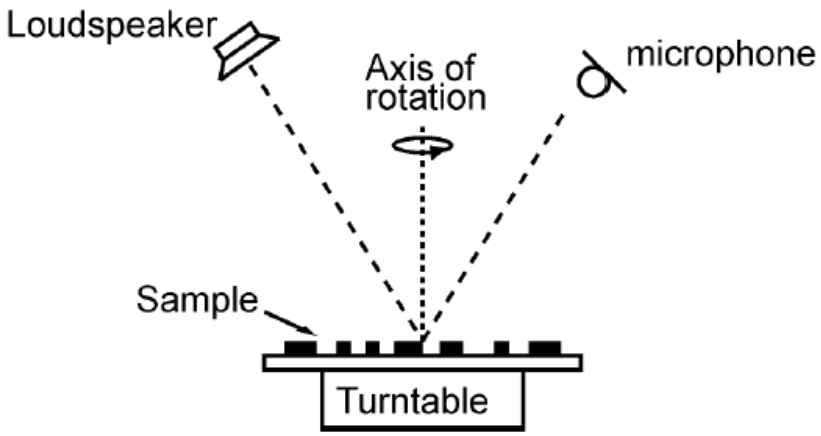

Figure 7.2: *Experimental set up for determining the specular reflected energy.*

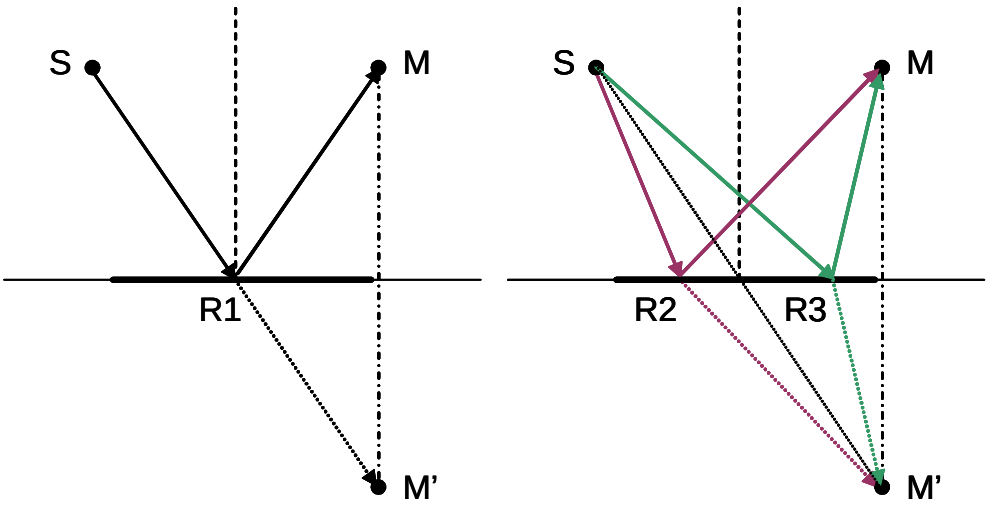

Figure 7.3: *The black rectangle represents a scattering surface with, on the left side, the specular reflection path shown. On the rigth, two reflection paths other than the specular path are shown.*

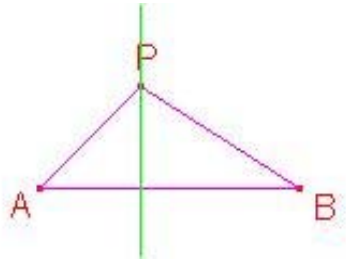

Figure 7.4: *Triangle illustrating the triangular inequality.*

This means that in figure 7.3

$$\left|SM'\right| < |SR2| + \left|M'R2\right| \tag{7.9}$$

and

$$\left|SM'\right| < |SR3| + \left|M'R3\right|. \tag{7.10}$$

This inequality holds for every reflection point R on the sample other than $R1$. So, the pathlength of the specular reflection will always be the shortest and thus the specular reflection will be the first reflection to arrive at the microphone. The specular reflected energy is found by phase lock averaging the reflected pressures while rotating the sample. This way the scattered components will average to zero and only the specular energy will remain. α_{spec} can be calculated using equation 7.4 ($\alpha_{spec} = 1 - E_{spec}$).

From equations 7.4 and 7.6 the scattering coefficient can be determined and reads:

$$s = 1 - \frac{E_{spec}}{E_{total}} = 1 - R_{spec} = \frac{\alpha_{spec} - \alpha}{1 - \alpha}, \tag{7.11}$$

with R_{spec} the specular reflected energy ratio given by $\frac{E_{spec}}{E_{total}}$.

It is also possible to predict the scattering coefficient for Schroeder diffusers by calculating the specular reflection coefficient, R_{spec}. The derivation goes as follows: by substituting equation 4.17 for the reflectivity of the wells in equation 4.10, the pressure scattered from a (Schroeder) surface into a certain direction θ is obtained which reads [9]:

$$p(\theta, \psi) \approx C \sum_{np=1}^{N_p} \sum_{n=1}^{N} e^{-2jkd_n} e^{jkx[\sin(\theta)+\sin(\psi)]}$$

Here C is a constant, N_p is the number of periods, N is the number of wells in a period, k the wavenumber, d_n the depth of the nth well, ψ the angle of incidence and θ the angle of reflection. The specular reflection energy can be found at $\psi = -\theta$

$$E_{spec} \approx \left| C' \sum_{np=1}^{N_p} \sum_{n=1}^{N} e^{-2jkd_n} \right|^2, \tag{7.12}$$

where C' is a constant. The specular reflection coefficient can be found by normalizing equation 7.12 with the energy from a flat plane surface and reads:

$$R_{spec} = \frac{\left| C' \sum_{np=1}^{N_p} \sum_{n=1}^{N} e^{-2jkd_n} \right|^2}{|C'N_pN|^2} = \left| \frac{1}{N} \sum_{n=1}^{N} e^{-2jkd_n} \right|^2 \tag{7.13}$$

Equation 7.13 represents the fraction of energy that is reflected in a specular manner by the scattering surface and, hence, the scattering coefficient can be evaluated with:

$$s = 1 - \left| \frac{1}{N} \sum_{n=1}^{N} e^{-2jkd_n} \right|^2 \tag{7.14}$$

Equation 7.14 is used to predict the scattering coefficient for the diffuser modelled in this research. The result is shown in figure 7.5. As can be seen the scattering coefficient varies between 0.7 and 1, indicating a good diffusive quality. There are three large dips at about 600, 2100 and $4000\,\mathrm{Hz}$ respectively. This means that at these frequencies more energy is reflected into the specular reflection direction than at the other frequencies.

The diffusion coefficient is generally considered a more strict test for diffuser quality than the scattering coefficient. This will be illustrated with an example. Consider a surface that scatters sound energy in one particular direction that is not the specular reflection direction, see figure 7.6. In this case the polar response will have an energy lobe in one particular direction and consequently equation 7.3 will produce a low value for the diffusion coefficient, on the contrary, the scattering coefficient will have a high value. This should be taken into consideration when working with the coefficients. More information can be found in [9].

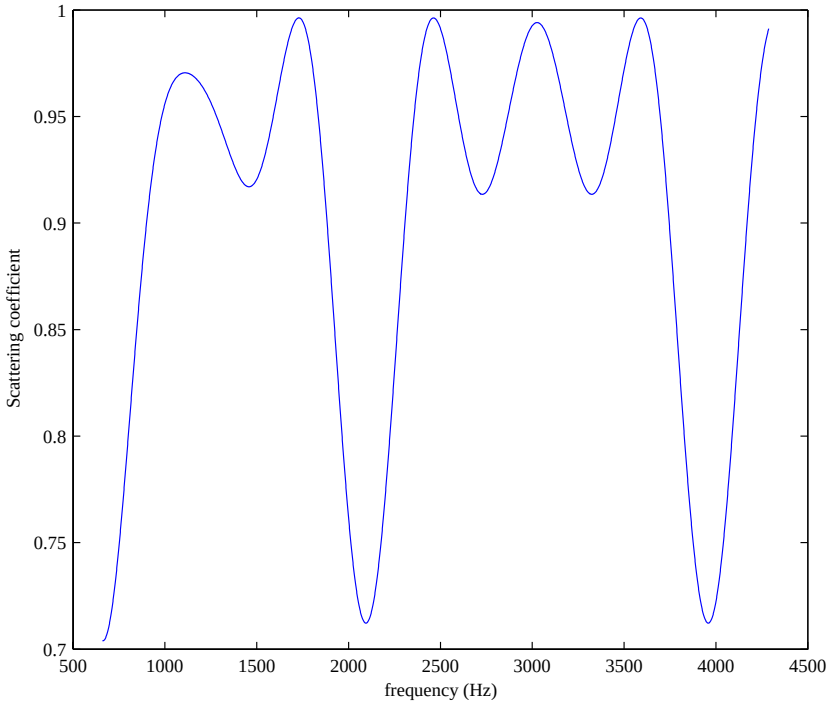

Figure 7.5: *The scattering coefficient as a function of frequency for the diffuser modelled in this research.*

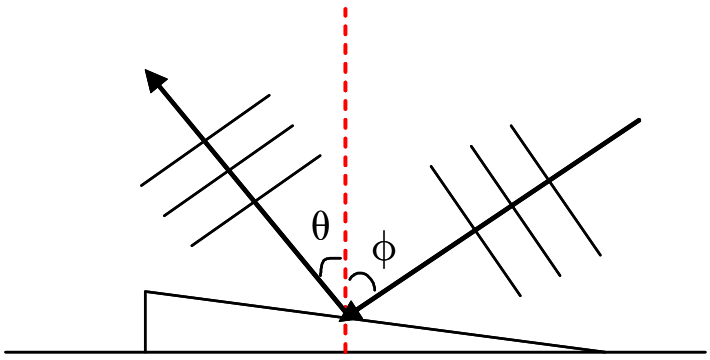

Figure 7.6: *Scattering surface with a low diffusion coefficient, but a high scattering coefficient. ϕ is the angle of incidence and θ the scattering angle.*

Chapter 7: The scattering coefficient

During the writing of this thesis the scattering coefficient has been calculated for the different hallway configurations discussed in this thesis. These configurations include the hallway with both the fuse box and the closet present and the hallway with the QRD and the closet present; the coefficient has also been calculated for the hallway without fuse box, closet and QRD. The results can be found in [17].

Chapter 8
Conclusions and recommendations

8.1 Conclusions

The image altering method of Kuster [1] to study the effects of boundary changes on 2D-array impulse responses has been succesfully applied to a QRD. In designing a QRD, there are two lower frequency criteria and two upper frequency criteria that determine its effective bandwidth. Which one of the lower and upper criteria determine the frequency range for which the diffuser effectively scatters, depends on the most important design parameter, which can be either the depth of the wells or the period length of the diffuser (which is dependent on the width of the wells). And thus, the effective frequency range can be altered using the two criteria that determine the bandwidth. In this research the requirement that there must be at least two scatter directions ($f_{\mathrm{min}}^{(2)}$) and the requirement that the width b of the wells must be smaller than the shortest apparent wavelength for which the diffuser is designed ($f_{\mathrm{max}}^{(2)}$), defined the effective frequency range for the diffuser that was modelled.

The sharpness (or resolution) of the image is determined by the resolution of the used source wavelet and cannot be higher than this resolution. Therefore, the diffuser has been modelled using this wavelet. The geometry of the diffuser required a resampling of the original image, because of the low amount of image points. As a consequence of the resulting high resolution a fast processor and sufficient memory are necessary; especially for the generation of the three-dimensional image.

Because of the presence of the diffuser in the hallway, the arrival times of the reflections at the array coming from the diffuser are more (discontinuously) spread in the lateral direction compared to the hallway with a flat wall between the columns, as was visible in the impulse responses of the

hallway. These different arrival times cause binaural dissimilarity leading to a stereophonic sound experience for the listener. Listening tests have been performed with a speech and a noise signal to check if the presence of the diffuser was really audible.

The overall outcome of the listening tests is that the presence of the diffuser is clearly audible for different energy ratios of the samples. However, in the case of the speech signal it was more difficult to hear the difference. On the other hand, in the case of the speech signal it was surprising that at a high energy difference the fraction of correct answers was relatively low. There has also been a study of two other measures for the amount of wrong answers. The relation between the amount of wrong answers and the energy ratio of the signals arriving at the left and the right ear has been studied. And because of the fact that the audibility of the presence of a diffuser is based on the effect of binaural dissimilarity, the correlation of the signals arriving at left and right ear has been calculated and the relation between the amount of wrong answers and the difference of this correlation in the case of hallway with and without the diffuser has been studied. Neither of these measures resulted in a better measure than the energy ratio of the samples in the case of hallway with and without the diffuser.

The amount of wrong answers at positions that are similar with listening positions in Kuster's test has been compared with the amount of wrong answers in Kuster's test. For these positions the amount of wrong answers was always larger in Kuster's test, indicating that the presence of the diffuser was better audible than the presence of the fuse box.

The diffusion coefficient and the scattering coefficient are two measures that define how well objects scatter sound, as explained in chapter 7. The scattering coefficient is a measure for the amount of energy that scatters away from *one* particular direction (the specular reflection direction), whereas the diffusion coefficient compares the polar response with a uniform distribution. According to these definitions a surface that scatters sound in one particular direction that is not the specular direction would give a high scattering and a

low diffusion coefficient respectively. This makes the diffusion coefficient a better measure for the diffusibility of objects.

The scattering coefficient for Schroeder diffusers can be predicted by calculating the specular reflected energy. This has been done for the modelled diffuser with the result that within the effective frequency range the scattering coefficient varies between 0.7 and 1, indicating a good diffusive quality.

8.2 Further research

The conclusions of this research left some points for further research. The diffuser modelled in this research has a specific effective frequency range. This can be altered, using the criteria given in this research, resulting in a diffuser with, for example, a different geometry or a diffuser on which sound impinges from a different direction. Next, the acoustical differences between the different diffusers can be studied by, for example, performing listening tests. The image-altering method used in this research creates the opportunity to compare different kinds of diffusers (two- and three-dimensional diffusers and diffusers modelled according to different algorithms) or other scattering objects, without having to build a physical model, and eventually make some kind of manual with these objects and their ability to scatter sound.

In the listening test in this research there was only one position that was exactly similar to a listening position in Kuster's test and three with $5\,\mathrm{cm}$ difference with positions in Kuster's test. The amount of wrong answers at these positions was always larger in Kuster's research which indicates that the difference between diffuser and no diffuser was better audible than fuse box and no fuse box. However, a better comparison can be made when there are more corresponding listening positions which is recommended for future studies.

It would be convenient if a measure could be given to the diffuser that indicates how well it scatters sound. There already exist two measures to indicate the diffusibility of a diffuser, namely, the diffusion coefficient and the

scattering coefficient. The diffusion coefficient measures the quality of the reflections by measuring the similarity between the scattered polar response and a uniform distribution. The scattering coefficient is a measure of the amount of sound scattered away from a particular direction, for example the specular reflection direction. At TU Delft, a research has been started in which these coefficients are being calculated for different objects in the hallway (closet, fuse box and eventually the diffuser modelled in this research). These coefficients can be used in combination with the manual described above.

The image-altering method based on wave field extrapolation is a method mostly used in seismics. It can now also be used in room acoustic design to calculate the wave field in a room or space and make more accurate predictions of the acoustical consequences of a specific geometry of the room or space.

Appendix A
The second low frequency criterion

In section 4.2.2 was shown that for at least two scattering directions

$$f_{\min} = \frac{\pm c}{L\left(\pm 1 + \sin\psi\right)} \tag{A.1}$$

Now, because of the fact that $f > 0$, for $\sin\theta_m = 1$ m can only be $+1$ and equation A.1 becomes

$$f = \frac{c}{L(1 + \sin\psi)} \tag{A.2}$$

For $\sin\theta_m = -1$ m will be -1 and equation A.1 becomes

$$f = \frac{c}{L(1 - \sin\psi)} \tag{A.3}$$

This leads to a criterion for $m = 1$ of

$$f_{\min}^{(2)} \geq \frac{c}{L(1 + \sin\psi)} \tag{A.4}$$

or for $m = -1$

$$f_{\min}^{(2)} \geq \frac{c}{L(1 - \sin\psi)}. \tag{A.5}$$

As can be seen from equations A.4 and A.5, for positive angles of incidence equation A.4 gives the lowest value for $f_{\min}^2$ and thus at this $f_{\min}^2$ the scattering angle for $m = 1$ shall be the first to appear. For negative angles of incidence equation A.5 gives the lowest value for $f_{\min}^2$ meaning that the scattering angle for $m = -1$ is the first to appear. So the second low frequency criterion is dependent on the angle of incidence and has the following form:

$$f_{\min}^{(2)} \geq \frac{c}{L(1 \pm \sin\psi)} \tag{A.6}$$

where the $+$ should be chosen for positive angles of incidence and the $-$ for negative angles of incidence.

References

[1] Kuster, M., *Acoustic reflection imaging in enclosed spaces*, paper accepted for publication in J. Acoust. Soc. Am.

[2] Berkhout, A.J., *Seismic migration*, Elsevier, 1982.

[3] Schroeder, M.R., *Binaural dissimilarity and optimum ceilings for concert halls: More lateral sound diffusion,* J. Acoust. Soc. Am, vol **65**(4), April 1979.

[4] D'Antonio, P. and Cox, T.J., *Two decades of sound diffuser design and development. Part1: Applications and Design*, J. Audio Eng. Soc., vol **46**(11), November 1998.

[5] Schroeder, M.R., *Diffuse Sound Reflection by maximum length sequences*, JASA, vol **57**(1), January 1975.

[6] Cox, T.J. and Lam, Y.W., *Prediction and evaluation of the scattering from quadratic residue diffusers*, J. Acoust. Soc. Am, vol **95**(1), January 1994.

[7] Schroeder, M.R., *Progress in Architectural Acoustics and Artificial Reverberation: Concert Hall Acoustics and Number Theory,* J. Audio Eng. Soc., vol **32**(4), April 1984.

[8] Berkhout, A.J., van Wulfften Palthe, D.W. and De Vries, D., *Theory of optimal plane diffusers*, J. Acoust. Soc. Am, vol **65**(5), May 1979.

[9] Cox, T.J. and D'Antonio, P., *Acoustic absorbers and Diffusers. Theory, Design and Application*, Spon Press, London, 2004.

[10] Schroeder, M.R., *Number Theory in Science and Communication*, Springer-Verlag Berlin Heidelberg, Germany, 1986.

[11] Schroeder, M.R. and Gerlach, R. E., *Diffuse Sound Reflection Surfaces*, 9th ICA, Madrid, Paper D8, 1977.

[12] Weisstein, E.W., *"Wiener-Khinchin Theorem",* From MathWorld–A Wolfram, Web Resource: http://mathworld.wolfram.com/Wiener-KhinchinTheorem.html.

[13] Berkhout, A.J., *Seismic Migration*, Elsevier, Amsterdam, 1982.

[14] Hargreaves, T.J., Cox, T.J. and Lam, Y.W., *Surface diffusion coefficients for*

room acoustics: Free field measures, J. Acoust. Soc. Am., vol **108**(4), October 2000.

[15] Hargreaves, T.J., *Acoustic diffusion and scattering coefficients for room surfaces*, Ph.D. Thesis University of Salford, 2000.

[16] Weisstein, E.W., *"Triangle Inequality"*, From MathWorld–A Wolfram, Web Resource: http://mathworld.wolfram.com/TriangleInequality.html

[17] De Vries, D., Joeman, N. and Schreurs, E., *Measurement-based simulation and analysis of scattering structures*, paper presented at Forum Acousticum 2005, Budapest, 2005.